Reconstruction of UV radiation: UV exposure of the Arcto-Norwegian cod egg population, 1957-2005

Master Thesis Meteorology

Brynhild Berge Sjølingstad

June 2007

Geophysical Institute
University of Bergen
Norway

Picture on the front cover shows
a cod egg in the last part
of the egg stadium.
Picture found at imr.no (2007).

Preface

First of all many thanks to my supervisors Jan Asle Olseth and Jochen Reuder at the Geophysical Institute, and Svein Sundby at the Institute for Marine Research for having the patience and time to assist me through this task. It has been an inspiring cooperation with an impressive devotion and enthusiasm at our meetings.

Also very special thanks to

-Marius for providing food, motivation and love every day.

-My parents for giving me creativity and a really good sense of humor :)

-Camilla, Kristian, my dad and all other contributors for helping me polish this masterpiece.

...and last but not least my fellow students at ODD and the Geophysical institute. The past years have been great! I never imagined being a weather-geek would be so enjoyable!:)

Contents

Chapter 1

Introduction

In the mid 70s Chlorofluorocarbons (CFCs), haloalkanes frequently used in industry, were proposed to cause ozone depletion (Crutzen, 1974; Molina and Rowland, 1974). Few years later, in the mid 80s, an ozone hole was reported over Antarctica (Farman et al., 1985). Consequently political act was taken to phase out the production of substances harmful to the ozone layer by an international treaty known as the Montreal protocol. The monitoring of ozone became of particular interest, leading to the 1985-publishing of the first conclusive evidence for a downward trend in ozone levels as spring ozone values over the Antarctica was reported to have declined by 40 % between 1975-1984 (Kerr and McElroy, 1993). Research linked an increase in UV radiation as a consequence of ozone depletion (Madronich et al., 1998), and the potential of a connection between UV radiation and detrimental effects to human health as increased risk of skin cancer was pointed out (Cascinelli and Marchesini, 1989). Ever since there has been an increasing interest in the links between the ozone layer, UV radiation and its impact on life at the surface of the earth.

One problem related to research on UV radiation is that accurate and systematic GUV (ground-based UV) measurements did not start until around 1990 and series for looking at trends are consequently short in length. Effort has therefore been made to develop ways of reconstructing UV radiation. To achieve calculations with a satisfactory temporal and spatial resolution, different models are used, where they commonly are based on radiation transfer calculations of various complexity (Ricchiazzi et al., 1998). As surface levels of UV radiation generally depend on certain astronomic, atmospheric and surface parameters some models solve algorithms with detailed information on these parameters. The model used for this study, STAR (Reuder and Koepke, 2005; Ruggaber et al., 1994), is one of them. To achieve more correct description of radiation conditions when a broken cloud cover is present, it is common to exploit the knowledge of the relationship between global radiation, clouds and UV. The accessibility of such data combination is in most cases poor, and as there are no global radiation measurements for the areas in this study the modelling runs with cloud data only.

The study of the effect of UV radiation on organic life on earth was first typically dominated by the effects on human health. But the focus quickly expanded to include reaction of the plants, other surface organism and in the later years also aquatic or-

ganism, particularly those present in the euphotic zone. Studies on the latter are not very abundant, but increasing. Several of them indicate that today's level of UV-B radiation is potentially harmful to aquatic organisms as cod eggs (Häder et al., 1998; Kouwenberg et al., 1999a,b).

A species relevant to this scientific area is the Arcto-Norwegian cod. The Arcto-Norwegian cod is a deep water fish with the Barents Sea as its feeding area. During winter the mature fraction of the population migrates southward from the feeding areas to the Norwegian coast to spawn. The spawning areas are located along a 1400 km long coastline with Lofoten as the main spawning area, the Møre spawning district to the south and the Finnmark spawning district to the north (Sundby and Nakken, 2007). Spawning takes place in the thermocline between the upper cool coastal water and the warmer Atlantic water below during March and April (Ellertsen et al., 1981). As the eggs are positively buoyant they ascend towards the upper layers within less than one day and are subsequently found at increasing concentration towards the surface (Sundby, 1991). Egg incubation time at the actual ambient temperature is about three weeks. During this period the eggs drift with the currents, and are vertically distributed depending on the wind-induced turbulent mixing (Sundby, 1983). During calm periods more than 90 % of the eggs are found above 10 m depth, while during strong wind mixing less than 20 % are found above 10 m depth (personal correspondence, Svein Sundby). Hence, exposure to UV radiation is highly variable both because of the variable cloud cover and because of the variable winds. After hatching, the larvae are able to control their vertical position by migration and they are normally found at highest concentrations between 10 and 30 m depth (Ellertsen et al., 1989). The period of the eggs, larvae and early juvenile stages, which includes the three first months of life, is a key period for growth and survival. After these three months the year class strength is mainly determined. The mortality is at its highest during the egg stage; thereafter it decreases exponentially (Sundby et al., 1989). It is assumed that the large egg mortality is mainly caused by predation, but exposure to UV radiation may potentially effect egg survival.

Although the number of studies of the effects of UV radiation on eggs of pelagic fish such as cod are increasing, there are presently no detailed quantitative investigations conducted on how UV radiation during this critical first stage might influence cod recruitment. In laboratory experiments (Kouwenberg et al., 1999a) and experiments in outdoor reservoir (Bèland et al., 1999), UV radiation (especially in the UV-B range) has shown to cause increased mortality of cod eggs. This would be impeding for the reproduction leading to a poorer recruitment to adult population (Bèland et al., 1999). However, existing studies also suggest that the cod eggs are insensitive to UV-B radiation (Kuhn et al., 2000; Skreslet et al., 2005), that there is an effect, but only under specific conditions which hardly ever occur (Eilertsen et al., 2007), or that the effect is positive in the way that UV-B reduce the amount of bacteria harmful for the eggs (Skreslet et al., 2005).

The contradictory results reflect the complexity of an estimation of the effects of UV radiation on aquatic organisms. This field is obviously very sensitive and not fully

understood. But as the cod in the critical first stadium spend several weeks in or near the sea surface, it is reasonable to assume that UV radiation has a potential influence.

The motivation of this study is therefore to reconstruct UV radiation and express the UV exposure of the Arcto-Norwegian cod egg population for 1957-2005 by developing a new method. The method express the amount of biological weighted radiation the cod egg population is exposed to, by considering vertical distribution of the cod eggs as a function of wind speed, and the transmissivity of UV radiation in sea water. The daily mean exposure is weighted according to the temporal distribution of egg concentration throughout the spawning period, and the yearly sum of the weighted daily values is expressed as a Cod Index. The biological weighting of the effects of UV radiation on cod eggs is described by a biological weighting function experimentally determined by Kouwenberg et al. (1999a). UV transmittance in sea water is approximated based on existing literature (Erga et al., 2005), while the vertical distribution of the cod eggs is calculated based on a formulae from Sundby (1983). In order to reconstruct UV radiation describing radiation in the whole spawning area, meteorological observations from six SYNOP stations (Svinøy, Vigra, Skrova, Andøya, Hekkingen and Torsvåg) are collected. Cod indices are calculated for each SYNOP station, and weighted according to the spatial and temporal distribution of the spawning to achieve the overall Cod Index for the Arcto Norwegian cod egg population.

To investigate the quality of the reconstructed UV radiation, reconstructed values is compared to observed values. Further, an investigation of the trends in UV radiation is an important part of the discussion. Also, trends in the Cod Indices for each station and overall Cod Index, in addition to what regulates the Cod Indices most, is discussed. Last, a comparison of the Cod Index to year class strength is conducted. If UV radiation induces cod egg mortality the variability in the Cod Index can be recognizable in the year class strength. The discussion also includes literature on how other parameters strongly regulate year class size. E.g. Ellertsen et al. (1989) showed that a high ambient sea temperature during the egg- and larval stage is a necessary but not sufficient condition for the formation of strong year classes. It has been hypothesized that a high temperature could be a proxy for the advection of plankton-rich Atlantic water masses (Sundby, 2000) which will increase the food abundance for the larvae. But high temperature might also be a proxy for other biotic and abiotic variables such as UV radiation. It is therefore important to keep in mind that biological systems are complex, and that the influence of one parameter may overshadow the effect of an other. Effects of UV radiation may therefore be difficult to recognize.

UV radiation in theory and the main parameters determining UV radiation reaching surface of the earth is presented in Chapter 2. In Chapter 3 the method for calculating the Cod Index is presented along with the data and literature used to describe the wind conditions, UV transmissivity in sea water, temporal and spatial distribution of the spawning and year class strength. Chapter 4 provides a description of the model used for reconstructing UV radiation and the collecting and processing of the input data. The results are described and discussed in Chapter 5, where the key aims are to compare reconstructed UV radiation to observed values, discuss trends in UV radiation,

evaluate the parameters in the Cod Index, look at the trends in the Cod Index, and compare the Cod Index to year class data to see if any correlation is present. Finally a summary and conclusion is given in Chapter 6.

This study is a contribution to the EU-project COST726 "Long term changes and climatology of UV radiation over Europe". The main objective of the project is to advance the understanding of UV radiation, determine UV radiation climatology and assess UV changes over Europe. The project is divided into four groups; Data collecting, UV-Modelling, Biological Effectiveness, Quality Control where this study will contribute with data to the former three.

Chapter 2

Ultra violet radiation

In this chapter some basic principles of Ultra Violet radiation (UV radiation) are presented. This includes the characteristics of UV radiation and the atmospheric processes related to UV radiation along with an overview of the factors determining UV radiation at the surface of the earth.

2.1 UV radiation

According to Figure 2.1 only a very small part of the solar radiation reaching the top of the atmosphere is UV radiation (200-400 nm). Nevertheless, as it is highly energetic radiation, it is capable of inducing significant photochemical and photobiological effects in the atmosphere and for living organisms on the surface of the earth.

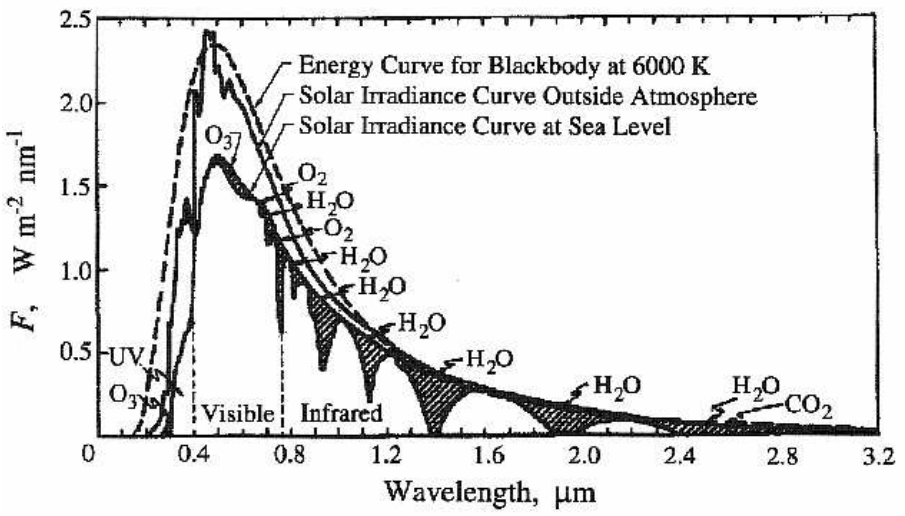

Figure 2.1: Clear sky spectral solar irradiance at sea level with sun in zenith, together with the similar irradiance outside the atmosphere. In addition, blackbody irradiance at 6000^o K is given (Figure from Seinfeld and Pandis (1998)).

The main atmospheric process, related to UV radiation, occurs in the lower part of the stratosphere. Here UV radiation causes a photodissosiation which breaks the bonds of

oxygen molecules(O_2) and forms ozone(O_3). Ozone absorbs most of the UV radiation which has not already been absorbed by atmospheric oxygen or ozone higher up in the atmosphere, especially the shortest and most energetic wavelengths. UV-C radiation (100-280 nm) is therefore essentially completely blocked. The atmospheric effect on UV radiation is seen in Figure 2.1. As ozone absorption is wavelength dependent, UV radiation with intermediate wavelengths, UV-B (280-315 nm), is only partly absorbed. While the shortest wavelengths, UV-A (315-400 nm) are weakly absorbed. The biological effects of UV-B radiation are the main focus of this paper, but with UV-A radiation included for some calculations.

2.2 Parameters effecting UV radiation

UV radiation at surface of the earth is very variable and depends on several conditions. One important factor effecting UV radiation, is the Rayleigh scattering. This is scattering of radiation by air molecules and occurs mainly for short wavelengths as the wavelength dependency is proportional to λ^{-4}. Rayleigh scattering is determined by the density of air molecules, and thus determined by the air pressure.

The remaining predominant variables determining UV radiation at surface of the earth are listed below.

- Solar elevation
- The total column of atmospheric ozone
- Cloud optical depth
- Albedo
- Turbidity

An example of how ozone and Solar zenith angle effect UV is shown in Figure 2.2, where the UV index is an irradiance scale computed by multiplying the CIE weighted irradiance in watts m^{-2} by 40 (http://woudc.ec.gc.ca, 2007). The UV index is a widely used measure of the effect of UV radiation on human skin.

2.2.1 Solar elevation

When the sun is close to the horizon, the solar radiation has to traverse a long distance trough the atmosphere before it reaches the surface, and the UV radiation is therefore considerably weakened by absorbtion and scattering. When the sun is close to zenith the solar radiation traverses a much shorter distance through the atmosphere, and the UV radiation is therefore less weakened. UV irradiances for different solar zenith angles are shown in Figure 2.2.

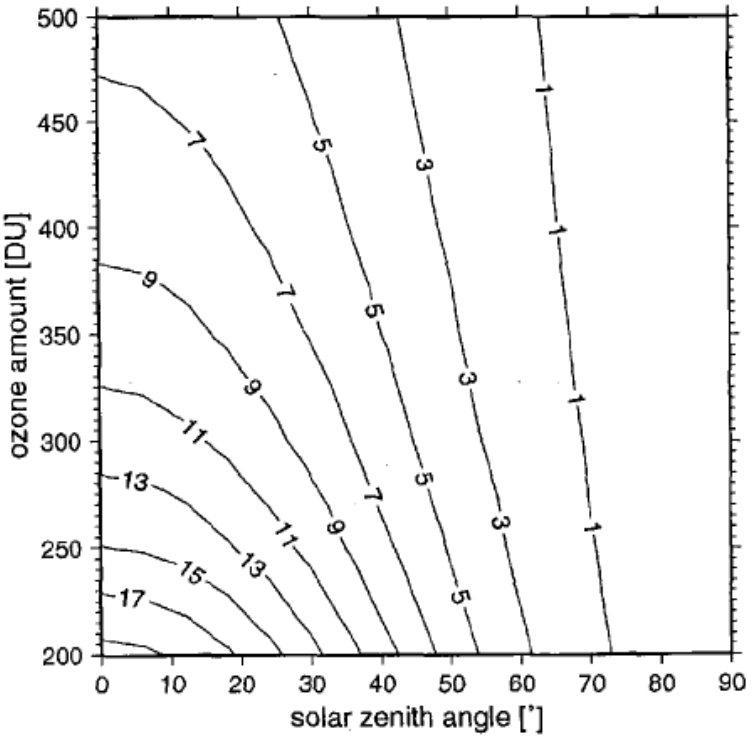

Figure 2.2: Erythemal weighted UV irradiance, given as UVI-isolines as a function of solar zenith angle and total ozone amount. (Figure from Koepke et al. (2002))

2.2.2 Total ozone

The total ozone amount is of great importance to UV radiation at surface (see Figure 2.2). The absorption of solar radiation of ozone starts at about 340 nm and increases toward shorter wavelengths, radiation with wavelength shorter than 200 nanometer is completely absorbed (Koepke et al., 2002). The absorption occurs in the photodissociation of oxygen molecules (Hartmann, 1994; Wallace and Hobbs, 1977).

$$O_2 + h\nu \quad \rightarrow \quad 2O \tag{2.1}$$

The atomic oxygen generated in this process is electronically excited and therefore highly reactive. In the stratosphere the concentration of this is high and often reacts with oxygen molecules to form ozone:

$$O_2 + O + M \quad \rightarrow \quad O_3 + M \tag{2.2}$$

This is the main reaction for Stratospheric ozone. UV radiation with wavelength between 200-320 nanometer is not strongly absorbed by the process of Equation 2.1, but instead it reacts with the ozone according to

$$O_3 + h\nu \quad \rightarrow \quad O_2 + O \tag{2.3}$$

Here the free oxygen atoms quickly recombine according to Equation 2.2 to form another ozone molecule.

Atmospheric ozone varies naturally with latitude and season (Svenøe, 2000). As the UV radiation is strongest in the tropical regions (Iqbal, 1983), the production of ozone is also largest here. But as UV radiation also destructs ozone, any accumulation of ozone is prevented. In addition there is a continuous transport of ozone towards the poles. At high latitudes ozone does accumulate. The UV radiation is weaker here and therefore little formation of ozone occurs. But the destruction is also low, so the high latitudes have the highes levels of ozone, with the exception of the Antarctica "ozone hole". As the total ozone column also varies with time of year it is essential to make regular measurements of the total ozone column.

Historically the most common ways of measuring ozone has been by ground instrumentation, but as technology evolves satellite based measurements are now common. The total amount of atmospheric ozone is usually given as Dobson Units (DU), where one Dobson unit is defined as the thickness 0.01 millimeter when the ozone column is compressed to the standard surface temperature and pressure (Svenøe, 2000).

2.2.3 Clouds

In contrast to ozone, which mainly absorbs UV radiation for wavelengths in the UV-B waveband and shorter (see Chapter 2.2.2 above), clouds decrease the surface irradiance both in the UV-A and UV-B area (Josefsson and Landelius, 2000; Schwander et al., 2002; Koepke et al., 2002). Under overcast conditions, reductions in UV radiation can exceed 90% (Bais and Lubin, 2007). The attenuation occurs because of multiple scattering within the cloud droplets. The scattering is defined by a scattering coefficient (Mayer et al., 1998; Koepke et al., 2002), and varies much with type (cloud cell morphology, particle size distribution and phase), amount and level of clouds. The high and thin clouds are relatively transparent for UV radiation, while low or medium thick clouds can be very opaque (Hartmann, 1994). For some conditions, particularly under optically thick clouds, multiple scattering can lead to enhanced absorption within the clouds because the scattering increases the path length (Mayer et al., 1998).

A common challenge connected to modelling of UV radiation is to calculate the real effect when a broken cloud cover is present. In spite of a large cloud fraction, the reduction in irradiance can be small if the clouds do not obscure the direct beam. Because of the complexities of cloud geometry it is very difficult to quantify the cloud effects in sufficient detail and this can bring variability and uncertainty into the calculation of the attenuation of the UV radiation (Josefsson and Landelius, 2000; Olseth and Skartveit, 1993).

2.2.4 Turbidity

The turbidity of the atmosphere expresses the efficiency of scattering and/or absorption of radiation by aerosols, small particles suspended in air. Aerosol attenuation of UV radiation is determined by optical parameters such as the spectrally dependent extinction coefficient $\beta(z)$ and the aerosol optical depth (AOD, shown in Equation 2.4), which is the vertical integral of the extinction coefficient.

$$AOD = \int \beta(z)dz \tag{2.4}$$

AOD also reflects the aerosol optical dependency of the relative humidity because increasing humidity causes swelling of aerosol particles.

The magnitude of the aerosol effect is highly variable, depending on the amount and on the physical and chemical composition (e.g., sulfate haze, soot, dust, sea-salt). However, differences in aerosol effect on UV radiation are mostly governed by differences in the aerosol amount (Koepke et al., 2002), which may vary strongly for different geographical locations (Reuder and Schwander, 1999). With an increase in the scattering and/or absorption of the atmospheric aerosols, UV radiation at surface of the earth will decrease. A sensitivity study by numerical modelling has shown that potential day to day variability in atmospheric aerosols may cause changes of spectrally integrated UV radiation quantities of 20 to 45 % (Reuder and Schwander, 1999). Several measurements of the decrease of UV radiation under turbid compared to clean conditions support this (Koepke et al., 2002; Reuder and Schwander, 1999). According to a study by Madronich et al. (1998) anthropogenic sulfate aerosols have decreased surface UV-B irradiances by 5-18 % in industrialized areas on the Northern Hemisphere, while measurements under variable pollution in Athens, showed a decrease in UV-B radiation of as much as 40 % (Koepke et al., 2002).

2.2.5 Albedo

Table 2.1: Local albedo values in the UV spectral range for various surfaces. Table from Koepke et al. (2002)

surface type	albedo	**surface type**	albedo
vegetation	0.01-0.07	**asphalt, concrete**	0.05-0.20
water	0.02-0.07	**granite**	0.30-0.45
bare soil	0.03-0.08	**old (wet) snow**	0.60-0.80
sand	0.04-0.30	**fresh snow**	0.80-0.98

The albedo of natural surfaces are well studied, and some of them are shown in Table 2.1. Reflections from the surface enhance upward radiation and because of multiple scattering and reflection in atmospheric components, like clouds and aerosols, this also enhances UV radiation at surface level (Reuder and Koepke, 2005). A field campaign at the salt lake Salar de Uyuni in Bolivia (albedo of ≈ 0.69) showed a distinct enhancement in UV levels compared to areas outside the lake. Measurements of the UV index showed 20 % higher values close to the center of the lake compared to measurements

outside the lake (Reuder et al., 2007).

Most of the natural surfaces in Table 2.1 have an albedo far below 0.1 in the UV spectral range, but as shown on the right side of Table 2.1, snow makes a distinct exception. Information of snow or ice cover is therefore important when looking at radiation over surfaces on land.

Chapter 3

Cod Index for the Arcto-Norwegian cod egg population

This chapter provides a description of the biological source of the cod eggs, the spawning behaviour, and results from some of the existing studies of the effect of UV radiation on cod eggs. Also, as one of the main goals of this study, a method for calculating a Cod Index - a measure of how the cod eggs are affected by UV radiation - is presented. The description of the Cod Index includes a presentation of the main components affecting the index and the argumentation for the use of them. But first of all, an overview of the geographical areas of interest in this study is given.

3.1 Study area

The geographical focus of this study is the spawning areas of the Arcto-Norwegian Cod. These areas are indicated with grey areas in Figure 3.1. The letters A-F simply refer to each individual spawning area where the spatial and temporal characteristic is unique for each area. This will be further discussed in Chapter 3.4.4.

The modelling of UV radiation for the spawning area requires relevant input data, i.e. a description of the atmospheric conditions within the spawning area. Weather stations of The Norwegian Meteorological Institute (met.no, 2007) have provided observations of meteorological parameters from several locations in Norway, but the selection of observation stations within the spawning grounds with long time series, fulfilling the demand for detailed cloud information, is very limited. However, the coastal stations Svinøy, Vigra, Skrova, Hekkingen, Torsvåg and Andøya do provide a sufficient amount of information. The stations are located within three of the six spawning areas, as indicated in Figure 3.1. More information on the stations and input data for the model used for reconstructing UV radiation will be given in Chapter 4.

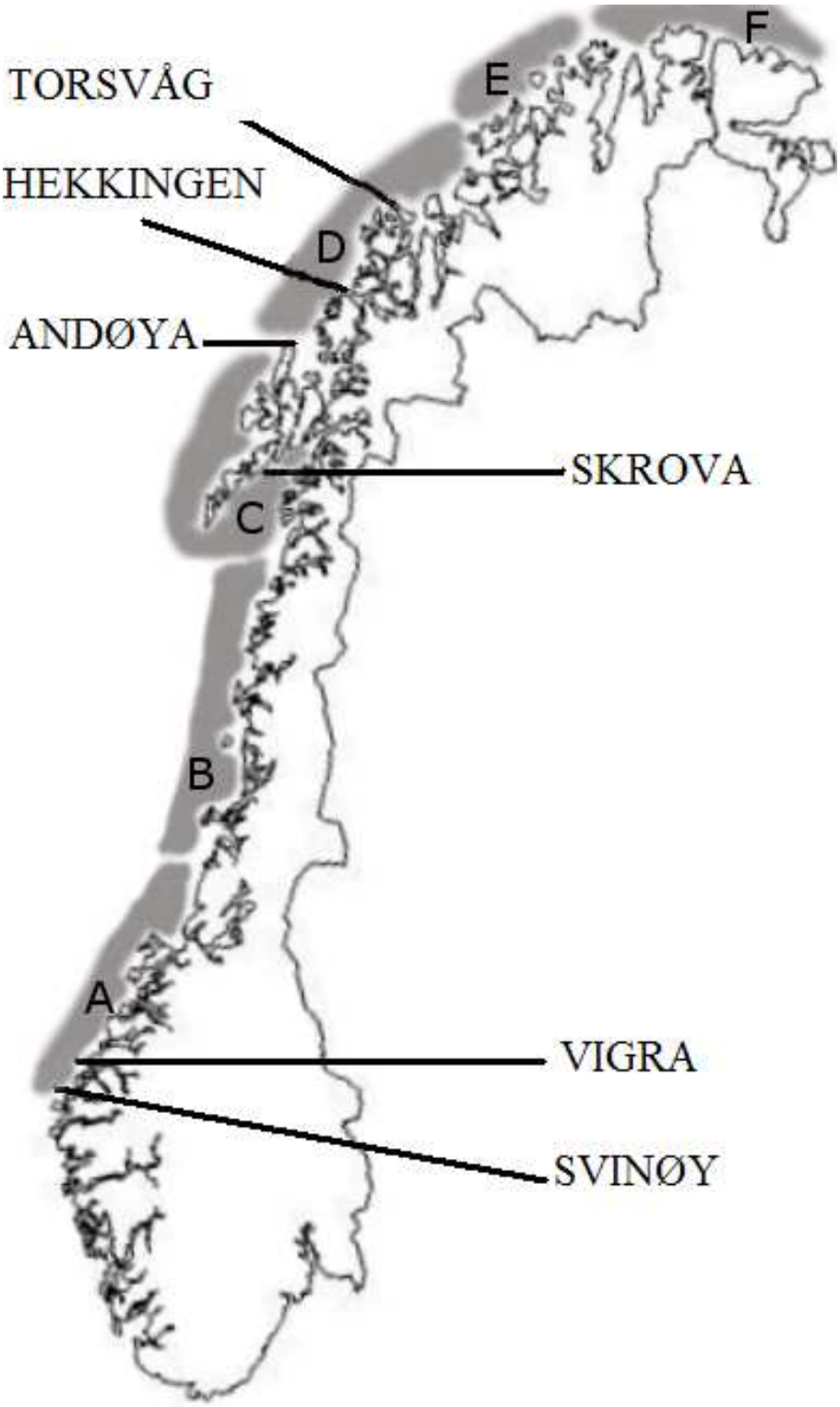

Figure 3.1: Geographical locations of spawning fields for Arcto-Norwegian cod (grey areas, A-F). Also indicated are the available SYNOP stations used in this study.

3.2 Arcto-Norwegian cod (Gadus Morhua)

The Arcto-Norwegian cod is a deep water fish with the Barents Sea as its feeding area. During winter the mature fraction of the population migrates southward from the feeding areas to the Norwegian coast to spawn. As indicated in Figure 3.1 the spawning areas are located along a 1400 km long coastline with Lofoten as the main spawning area, the Møre spawning district to the south and the Finnmark spawning district to the north (Sundby and Nakken, 2007).

Spawning of the Arcto-Norwegian cod starts in the beginning of March, peaks in the beginning of April, and ends in the beginning of May (Ellertsen et al., 1989). Although the spatial distribution has changed and typically moved northward as the sea temperature has increased during the last decades (Sundby and Nakken (2007); this will be further discussed in Chapter 3.4.4) the temporal distribution around the months of March and April is known to have been kept unchanged.

The eggs are spawned and fertilized at the depth of 50-200 meters in the thermocline between the upper cool coastal water and the warmer Atlantic water below (Ellertsen et al., 1981). As the eggs are positively buoyant they ascend towards the upper layers within less than one day and are subsequently found at increasing concentration towards the surface (Sundby, 1991). The egg stage last for about three weeks and in this period they drift along with the current or are mixed within the mixed layer according to the turbulent environment due to surface winds. Finally, they hatch after about 20 days and become larvae which actively prefer deeper layers (around 20 meters) (Bèland et al., 1999; Sundby, 1983).

The period of the egg, larvae and early juvenile stages, which includes the three first months of life, is a key period for growth and survival. After these three months the year class strength is mainly determined. The mortality is, however, at its highest during the egg stage (Sundby et al., 1989). It is assumed that the large egg mortality is mainly caused by predation. Potentially, however, exposure to UV radiation might also affect egg survival.

3.3 UV radiation effect on cod eggs

The cod eggs are subjected to a high mortality. Sundby et al. (1989) estimated that on the average only 10 % of the eggs hatch. It is assumed that egg predation is the main cause of the mortality. Predation from herring has been identified as an important mortality factor (Melle, 1985), but also gelatinous plankton is considered to be an important prey organism. However, also abiotic factors, such as UV radiation, might cause mortality.

Recent studies indicate detrimental effects of UV radiation on aquatic organisms as cod eggs (Häder et al., 1998; Bèland et al., 1999; Kouwenberg et al., 1999a,b). The

biological effect on Atlantic cod (Gadus Morhua) eggs by UV radiation is in Kouwenberg et al. (1999a) described by a biological weighting function (BWF) based on the knowledge of damage to the naked DNA in fish eggs. In this study, UV-B radiation for wavelengths 280-312 nm had a strong negative impact on the survival of cod eggs. There are, however, also studies which contradict the assertion of UV induced mortality in cod eggs (Kuhn et al., 2000; Eilertsen et al., 2007; UVAC project, 2003). In a recent study by Eilertsen et al. (2007) results showed that only under extreme meteorological conditions which seldom occur the exposure of UV is strong enough to cause a significant mortality. Also, in Skreslet et al. (2005) results indicated an indirect positive effect of UV radiation on the survival of the cod eggs, suggested to control harmful microbes. The conclusions are however, in many cases based on model studies or studies in laboratory or artificial environment. Studies on how UV radiation effects cod eggs in their natural environment are few in number.

Positive trends in UV radiation has been observed for the last decades at mid-latitude, so a corresponding increase in solar UV radiation penetrating the euphotic zone is assumed. This has led to an increase in UV exposure on cod eggs (Häder et al., 1998). If UV radiation induces mortality in cod eggs, the mortality could be possible to quantify by comparing the amount of radiation that a cod egg population is exposed to with the survival of cod eggs, i.e. the year class sizes. In the following Chapter 3.4 a method for calculating this is described using weighted radiation according to the BWF derived by Kouwenberg et al. (1999a). As Kouwenberg et al. (1999a) shows an insignificant effect in the UV-A area, the effects of cod weighted UV-B radiation will be the main focus of this study.

3.4 Method for calculating a Cod Index

One important aim of this study is to develop a Cod egg UV index (herafter called Cod Index) which quantifies the UV exposure on the cod egg population.

The index is calculated based on the following items:

- Biological weighted UV radiation at sea level, see Chapter 4for the reconstruction
- Transmission of UV radiation in sea water
- Vertical distribution of cod eggs
- Actual spawning period, Gauss distributed
- Spatial distribution of the spawning areas with data on the abundance of cod eggs/size of cod stock

3.4.1 Biologically weighted UV radiation

As mentioned in Chapter 3.3, damage by UV radiation on Atlantic cod is quantified by use of a BWF experimentally determined by Kouwenberg et al. (1999a). Field studies on eggs and larvae of cod in Austnesfjorden (Lofoten, area C in Figure 3.1) showed results comparable with the experiments of Kouwenberg et al. (1999a), the BWF is therefore assumed applicable for the study of Arcto Norwegian cod (Browman and Vetter, 2002).

The biological weighting coefficient $E_H(\lambda)$ from Kouwenberg et al. (1999a) for radiant exposure is shown below, in addition to a visual presentation in Figure 3.2.

$$E_H(\lambda) \quad = \quad C \cdot exp[-(m_1 + m_2(\lambda - 290))] \tag{3.1}$$

where m_1 and m_2 are fitted parameters and C(J m^{-2}) is a proportionality constant, here equal to one.

Kouwenberg et al. (1999a) observed a strong negative impact on the survival of Atlantic cod eggs for wavelengths below 312 nm, but no indications of an effect for wavelengths longer than 320 nm (UV-A radiation). In Figure 3.2 the weighting function for the UV-B region is shown in the left area. To include the possibility of an effect in the UV-A area it is in this study assumed that the curve for weighted radiation in the UV-B area decreases exponentially into the UV-A area, this is indicated in the right area of Figure 3.2.

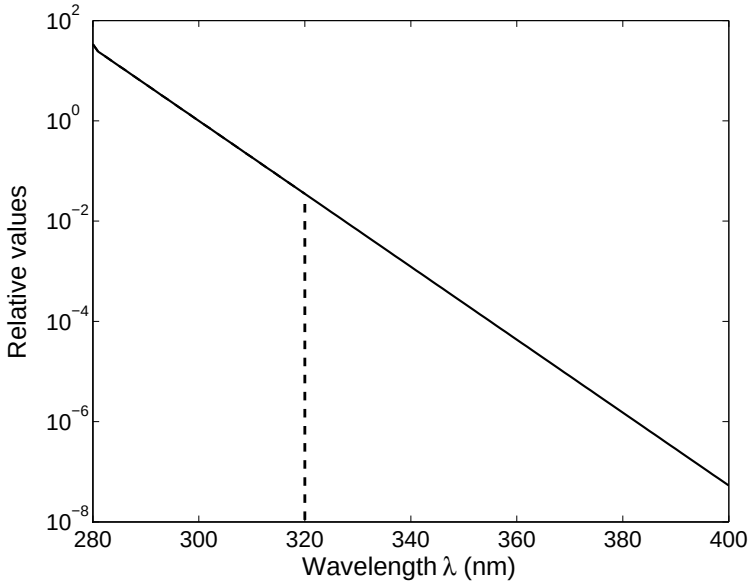

Figure 3.2: Biological weighting functions for cod eggs in the UV-B region (below 320 nm) based on data from Kouwenberg et al. (1999a). An extrapolation in the UV-A (above 320 nm) is also shown.

In Figure 3.3 modelled spectral irradiances for a cloud free day at Andøya are shown.

In addition, the cod weighting function is combined with the spectral irradiances to estimate biologically effective irradiance at each wavelength in the UV-B and UV-A area. The figure illustrates that wavelengths between 305-312 have the strongest effect on cod eggs and that the effect in the UV-A area is small.

Further calculations of the Cod Index in this study is conducted with cod weighted radiation in both the UV-B (CodUVB) area and for the total of UV-B and UV-A radiation (CodUVAB). The overall Cod Index for the Arcto-Norwegian cod egg population will however mainly be based on the assumption that effects of UV radiation on cod eggs are restrained to the UV-B waveband.

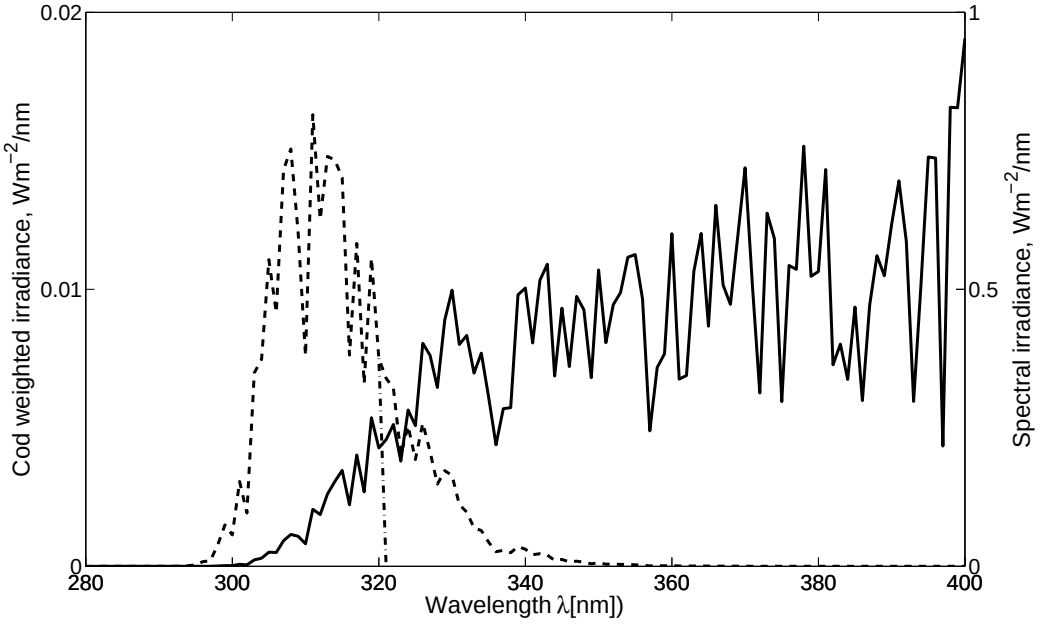

Figure 3.3: Modelled spectral irradiance (solid curve) for a cloud free day at Andøya (69.30°N 16.15°E); 29th of June 2003 at 12 UTC, total ozone column: 309 DU, aerosol profile: maritime clean (0.15). In addition, cod weighted UV-B radiation (below 320 nm) and cod weighted UV-AB radiation for the whole wavelength region (broken curves).

3.4.2 Transmission of UV radiation in water

Studies have shown that short wavelength radiation from the sun is able to reach ecologically significant depths in both fresh water and marine ecosystems (Häder et al., 1998). Information needed to estimate quantitatively UV damage on organisms distributed in the vertical therefore includes the spectral characteristics of solar radiation penetrating to depths.

Water transparency to electromagnetic radiation is characterized by Beers law

$$UV_z = UV_0 \times exp[-\kappa_d \ell] \tag{3.2}$$

where UV_z is the radiation at a certain depth z, UV_0 is the radiation at the sea surface, κ_d is the extinction coefficient (the sum of scattering and absorption of the direct beam of radiation), and ℓ is the distance that the radiation travels to depth z (path of extinction) (Wallace and Hobbs, 1977).

Light absorption and scattering in the ocean are strongly wavelength dependent. While light absorbtion in the visible region of the electromagnetic spectrum steeply decreases to a minimum at about 420 nm, absorption of $\lambda < 420$ nm steeply increases. Thus UV-A radiation and visible light are able to penetrate considerably larger depths than radiation in the UV-B area (Losey et al., 1998; Capone et al., 2002).

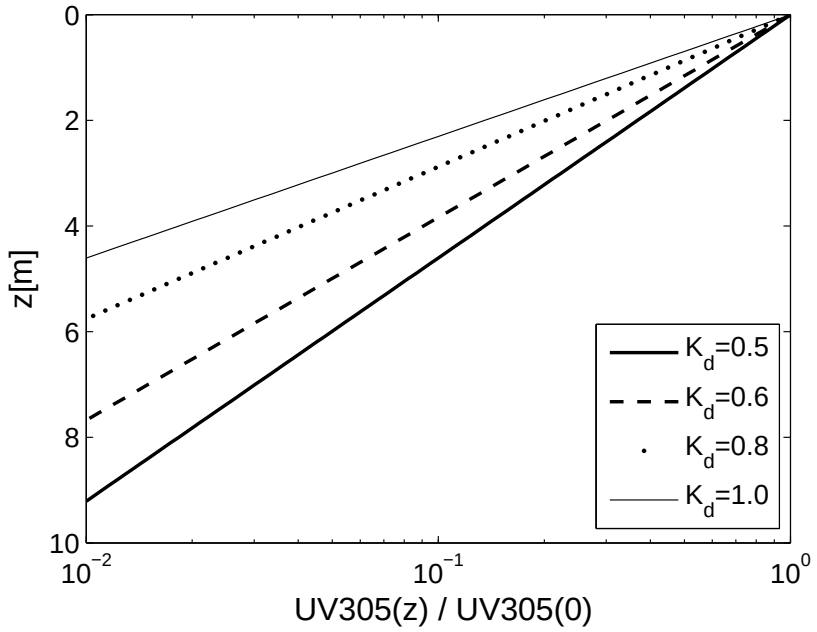

Figure 3.4: UV transmission (305 nm) of sea water calculated for various extinction coefficients K_d. Intersection with y-axis indicates depth where radiation is reduced to 1 % of surface level.

The amount of radiation reaching the depths depends on the optical properties of sea water as salinity, water temperature and inorganic matter (Capone et al., 2002). As the optical properties show large temporal and regional differences in different marine sites (Häder et al., 1998), in situ measurements are necessary to determine the exact transmission profile of radiation. There are, however, no specific measurements of these properties made especially for the locations of this study. Based on the study of Erga et al. (2005) on UV transmission in Norwegian marine waters as a basis, reasonable values for the transmissivity are possible to calculate. Erga et al. (2005) calculated the depths of four different wavelengths (305, 320, 340 and 380 nm) where the light is reduced to one percent of its surface value on a transect between Bear Island and

East Greenland. The measuring sites are oceanic, coastal and fjord locations. As the main interest is radiation in the UV-B area, the measurements for 305 nm are very representative for this work. The maximum penetration of UV-B radiation into the deep is found in the clear oceanic waters midway along the transect, but for the coastal locations most of the radiation is attenuated at 5-10 meters. According to Equation 3.2, the depth of 5-10 meters for the 99 % reduction in UV-B radiation will give an extinction coefficient κ_d of 0.5-1.0. The transmission profile for UV-B light of 305 nm is shown for various values of κ_d in Figure 3.4.

3.4.3 Vertical distribution of the cod eggs

To quantify the UV radiation exposure of cod eggs it is necessary to calculate the vertical distribution and displacement of cod eggs within the mixing layer (Kouwenberg et al., 1999a; Kuhn et al., 2000). This is dependent on the turbulence of the mixed layer which is mainly determined by the wind conditions. Obviously, for low wind speeds the egg concentration near surface is higher than for high wind speeds and the exposure to UV radiation is thus higher. Firstly, the method for calculating the distribution will be discussed, secondly, the wind data used for this work will be presented and discussed.

Formulae and Equations

The formulae used for the calculation of the vertical distribution of cod eggs is taken from Sundby (1983) and is frequently used in the mapping of egg production of pelagic fish eggs.

The formulae expresses the concentration of pelagic eggs at the depth z [m] and the wind speed u [ms^{-1}] as:

$$C(z,u) \quad = \quad C(0,u) \cdot exp[\tfrac{-w}{K(u)} \cdot z] \tag{3.3}$$

where K is the vertical eddy diffusivity coefficient [m^2s^{-1}], here presumed constant through the mixed layer and varying only as a function of the mean wind speed u.
w is the average vertical speed of the eggs due to positive buoyancy [ms^{-1}].
and C(0,u) is the egg concentration at the surface for a given wind speed u [m^{-3}] .

Field studies of pelagic fish eggs from various species have provided a relationship between the mean wind speed u and K, given as:

$$K(u) \quad = \quad (76.1 + 2.26u^2)10^{-4} \tag{3.4}$$

According to Equation 3.4, K is relatively large for u = 0, this is partly due to mixing caused by the tidal flow in coastal areas.

The ascending velocity of eggs toward the surface is dependent on the cod egg buoyancy and size (diameter). This varies with species, but also within the species. Combining

the results of several studies on Arcto-Norwegian Cod it is reasonable to use a mean speed of 0.001 m s^{-1} (personal correspondence, Svein Sundby).

For the further investigation a normalized concentration profile for cod eggs (C_N) has been developed.

$$C_N(z,u) = C_N(0,u) \cdot exp[\tfrac{-w}{K(u)} \cdot z] \tag{3.5}$$

By definition, the normalized surface egg concentration for wind conditions u=0 ms^{-1}, C_N(0,0), is set to 1.

The normalized number of cod eggs above a given depth z_1 for wind speed u=0 ms^{-1} (N_0) is given by:

$$N_0 = \int_0^{z_1} C_N(0,0) \cdot exp[\tfrac{-w}{K(0)} \cdot z]dz \tag{3.6}$$

the corresponding expression for wind speed u:

$$N_u = \int_0^{z_1} C_N(0,u) \cdot exp[\tfrac{-w}{K(u)} \cdot z]dz \tag{3.7}$$

Assuming that the total number of cod eggs has to be constant, independent of wind speed, Equations 3.6 and 3.7 can be used to define C_N(0,u) by:

$$C_N(0,u) = \frac{\int_0^{z_1} exp[\frac{-w}{K(0)}z]dz}{\int_0^{z_1} exp[\frac{-w}{K(u)}z)dz} \tag{3.8}$$

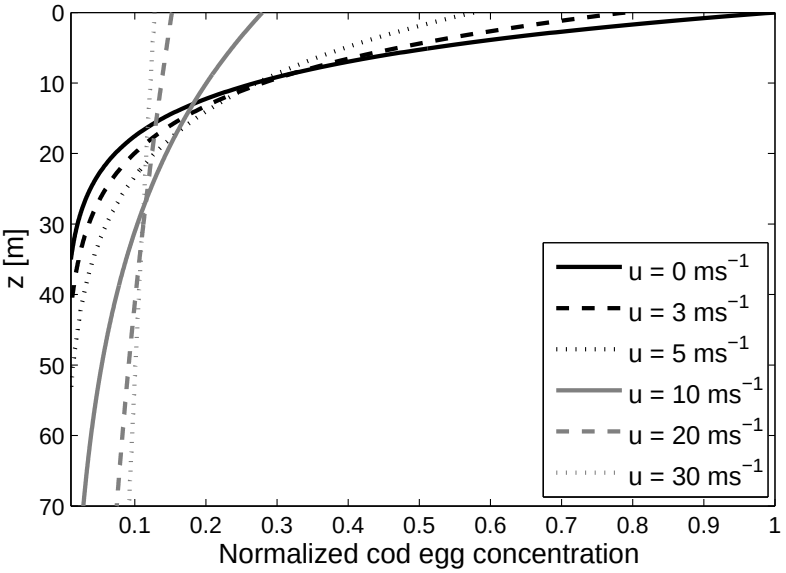

Figure 3.5: Normalized vertical distribution of cod eggs as a function of mean wind speed according to Equation 3.5. Shown for six different wind speeds (0-30 ms^{-1}).

where z_1 = -70 m. Very few cod eggs mix below this point, and therefore a cut-off depth is defined here (personal correspondence, Svein Sundby).

The integrals in Equation 3.8 above can be analytically expressed as:

$$\int_0^{z_1} exp(ax)dz \quad = \quad \tfrac{1}{a}exp(ax)|_0^{z_1} \tag{3.9}$$

For wind speed u, the integrals will thus be given by:

$$\begin{aligned} \int_0^{z_1} exp(-\frac{w}{K(u)}z)dz &= -\frac{K(u)}{w} \cdot exp(-\frac{w}{K(u)} \cdot z)|_0^{z_1} \\ = -\frac{K(u)}{w} \cdot exp(-\frac{w}{K(u)} \cdot z_1) &- [-\frac{K(u)}{w} \cdot exp(-\frac{w}{K(u)} \cdot 0)] \\ &= \frac{K(u)}{w}[1 - exp(-\frac{w}{K(u)} \cdot z_1)] \end{aligned} \tag{3.10}$$

Figure 3.5 shows the normalized vertical distribution of cod eggs as a function of wind speed according to Equation 3.5 and examplifies how the wind affects the vertical distribution of cod eggs. Due to the attenuation of UV radiation in sea water, cod egg exposure to UV radiation is considerably reduced for high wind speeds inducing mixing of the cod eggs deeper in the vertical. When most of the eggs lie near the surface the exposure to UV radiation is much stronger.

Wind data

Wind observations from the chosen SYNOP stations are not abundant for the actual time period. Further on, the observation sites are located on land, so in many cases the wind is affected by the surrounding vegetation and topography, which causes lee wind or turbulence. As the spawning areas mostly lie some distance off shore, the SYNOP data are for many cases less representative for the wind field than desired.

Alternatively, wind conditions are described by wind data from the Hindcast database, kindly provided by met.no. The Hindcast data are calculated based on pressure fields. With a resolution of 75 km it enables the descriptions of the wind conditions for the different spawning areas. Wind data were generated for four areas located at a certain distance off shore, but within a reasonable distance of the six stations. Individual wind data sets were generated for each of the stations Skrova and Torsvåg, but for Svinøy and Vigra in the south and Andøya and Hekkingen in the north the wind data were generated for two joint locations.

The Hindcast data set has a temporal resolution of six hours. To fit the needs of the calculations of the Cod Index, the data sets are extended to a temporal resolution of

one hour by using the data from the last data hour if no data are present.

Validation of Hindcast data

To justify the use of the Hindcast wind data a comparison of observed wind data and Hindcast wind is shown in Figure 3.6.

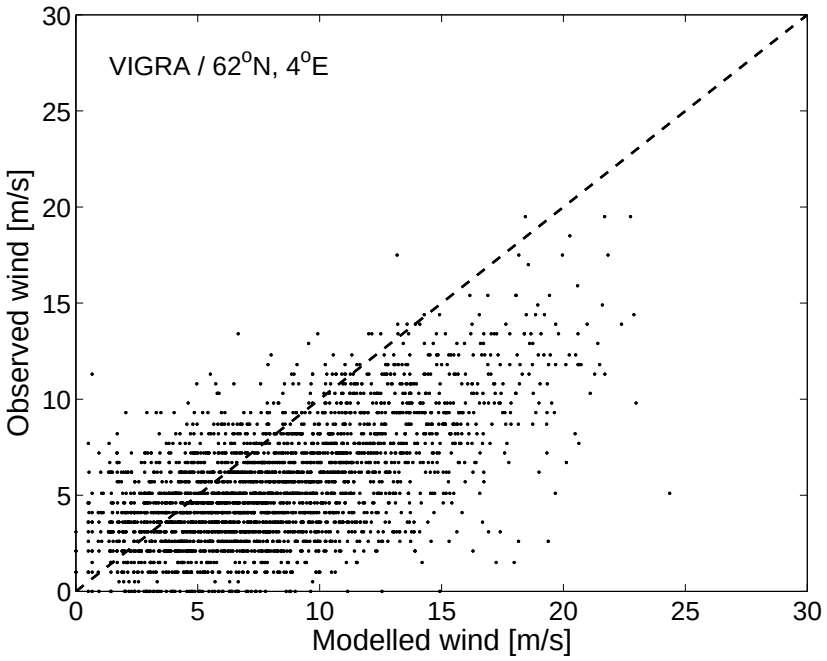

Figure 3.6: Observed wind at Vigra versus wind data from the Hindcast database for the offshore location 62^o N, 04^o E for 1969-1970.

As expected, the Hindcast data show overall higher values than the observed wind at the onshore stations. This was expected as the mountains and topography in general surrounding the SYNOP stations affect the observed wind, in many cases through sheltering effects (sharpening effects are though also possible for some wind directions). As the Hindcast data are calculated for locations at some distance from shore, the interfering effects are eliminated and the data are therefore believed to be the most correct data available for describing the wind conditions of the spawning areas.

It is, however, worth mentioning that despite the choice of not including information on the wind direction, the wind direction is not irrelevant. Spawning occurs offshore, but for some areas nearby mountains will have an effect on the wind for certain wind directions. High surrounding mountains in Lofoten will for example result in a high sea into Vestfjorden (located in area C in Figure 3.1) for southwesterly winds (Sundby, 1983). The wind direction and its effect are however not accounted for because of limited time available for this project. It should, however, be mentioned that this could be a potential source of error.

3.4.4 Spatial and temporal distribution of the spawning

Spawning areas

The work of monitoring and understanding the spawning behavior of Arcto-Norwegian cod has been ongoing for several years (Sundby, 1983; Sundby and Bratland, 1987). The 1400 km long coastal spawning area has been divided into smaller areas, visually shown in Figure 3.1. As described in Chapter 3.2 the spawning time has been constantly concentrated around March and April. The percentage distribution of the spawning on the six areas (Figure 3.1) has however varied from year to year. Information on this is provided by Svein Sundby and is shown below in Table 3.1 and in Figure 3.7. The table is based on an egg-survey from Northern Norway for the years 1983, 1984 and 1985. It is then adjusted to fit the time-development based on a study on how spawning areas have changed according to long term trends in the temperature (Sundby and Bratland, 1987).

Changes in the spawning activity are easily identified in Figure 3.7. The spawning activity in the south was essentially higher in southern areas (A and B) for the years 1960-1980 than for the years after 1980. This is believed to be because of variations in sea temperature. During the "cold" 1960s and 1970s the cod preferred southern areas, while after 1980 the sea temperature has in general increased and the cod now spawns further north (personal correspondence with Svein Sundby). It is worth noticing that the percentage of spawning occuring in the Lofoten area (area C) has remained almost unchanged, but during the last decade this area also seem to be effected by the northward immigration.

Future changes in the geographical distribution of the spawning area will be further discussed in Chapter 5.

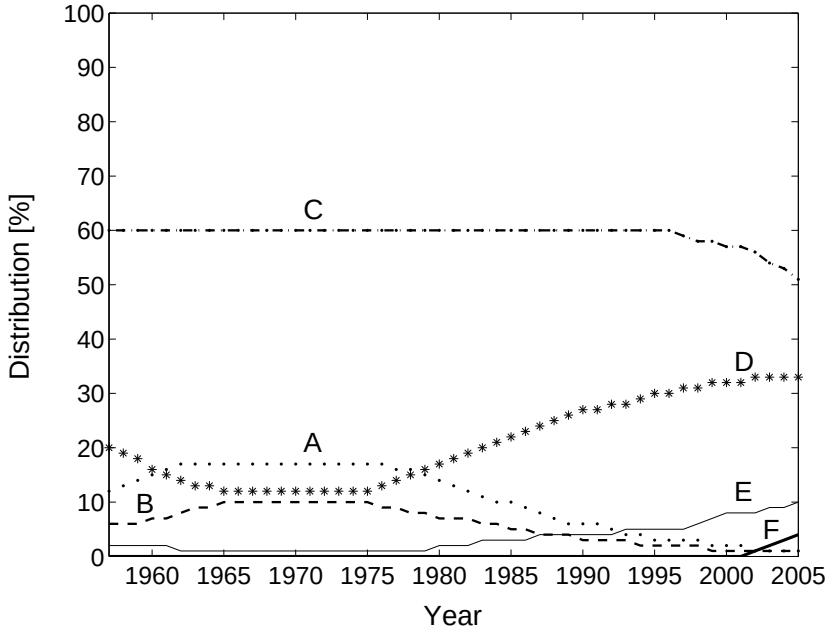

Figure 3.7: Distribution of spawning areas corresponding to Table 3.1

Table 3.1: Yearly percentage distribution of the spawning at following locations: A) The coast of Møre (Stadt-Trondheim), B) Helgeland (Rørvik-Bodø), C) Lofoten/Vesterålen (Bodø-Andenes), D) Troms (Andenes-Sørøya), E)Vest-Finnmark (Sørøya-Nordkapp, F) Øst-Finnmark (Nordkapp-Vardø). Numbers based on Sundby and Bratland (1987); Sundby and Nakken (2007), provided by Svein Sundby.

Year	A	B	C	D	E	F	**Year**	A	B	C	D	E	F
1957	10	5	60	22	3	0	**1982**	12	7	60	19	2	0
1958	11	5	60	21	3	0	**1983**	11	6	60	20	3	0
1959	12	6	60	20	2	0	**1984**	10	6	60	21	3	0
1960	13	6	60	19	2	0	**1985**	10	5	60	22	3	0
1961	14	6	60	18	2	0	**1986**	9	5	60	23	3	0
1962	15	7	60	16	2	0	**1987**	8	4	60	24	4	0
1963	16	7	60	15	2	0	**1988**	7	4	60	25	4	0
1964	17	8	60	14	1	0	**1989**	6	4	60	26	4	0
1965	17	9	60	13	1	0	**1990**	6	3	60	27	4	0
1966	17	9	60	13	1	0	**1991**	6	3	60	27	4	0
1967	17	10	60	12	1	0	**1992**	5	3	60	28	4	0
1968	17	10	60	12	1	0	**1993**	4	3	60	28	5	0
1969	17	10	60	12	1	0	**1994**	4	2	60	29	5	0
1970	17	10	60	12	1	0	**1995**	3	2	60	30	5	0
1971	17	10	60	12	1	0	**1996**	3	2	60	30	5	0
1972	17	10	60	12	1	0	**1997**	3	2	59	31	5	0
1973	17	10	60	12	1	0	**1998**	3	2	58	31	6	0
1974	17	10	60	12	1	0	**1999**	2	1	58	32	7	0
1975	17	10	60	12	1	0	**2000**	2	1	57	32	8	0
1976	17	9	60	13	1	0	**2001**	2	1	57	32	8	0
1977	16	9	60	14	1	0	**2002**	1	1	56	33	8	1
1978	16	8	60	15	1	0	**2003**	1	1	54	33	9	2
1979	15	8	60	16	1	0	**2004**	1	1	53	33	9	3
1980	14	7	60	17	2	0	**2005**	1	1	51	33	10	4
1981	13	7	60	18	2	0							

Temporal distribution within the spawning period

As the spawning of the Arcto-Norwegian cod is restrained to a fixed time period within the year (Chapter 3.2) it makes it possible to isolate and study closely the actual period when the cod eggs are exposed to radiation. It is however necessary to make a slight adjustment to the period of further interest.

According to Chapter 3.2 the spawning and fertilization start in the beginning of March, peak in the beginning of April, and end in the beginning of May. As the egg stage lasts for about three weeks, the peak in egg concentration is found about one and a half week after peak spawning. Hence, the time of interest with respect to UV exposure will be shifted 10 days to 10th of March - 10th of May (personal correspondence, Svein Sundby). Therefore, a Gaussian distribution (Figure 3.8) with its peak at 10th of April is chosen as a weighting function for all data believed to affect the UV exposure of the cod eggs.

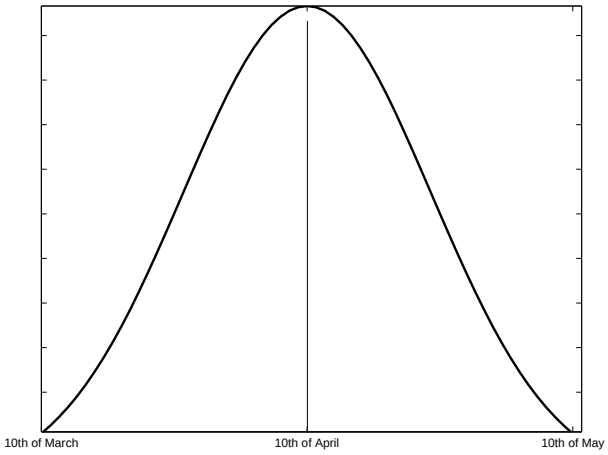

Figure 3.8: Gaussian distribution over 62 days (10th of March to 10th of May).

3.4.5 Overall Cod Index

The sections above presents the different variables used in the method for calculating a Cod Index. When data on radiation and wind conditions are achieved for locations relevant to the area of interest, the actual Cod Index per station is calculated by combining wind data and the UV transmission profile for sea water with radiative data. The daily values are Gaussian distributed, and summed to a yearly value. In this way relative values of UV exposure on cod eggs are presented.

UV radiation is reconstructed for six stations, so a Cod Index for each area is first calculated. Secondly, each station‘s yearly Cod Index must be combined with information of the temporal and spatial distribution of the spawning areas in Table 3.1. Ideally one station should represent one area, but as the different six stations from Figure 3.1 only lie within three of the current spawning areas (also indicated in the map) it is necessary

to merge some of the areas (shown in in Table 3.2). Thus, stations are combined to achieve a Cod Index representative for the whole area. At last, the yearly Cod Index per area is weighted according to the spawning distribution per area shown in Table 3.1 and summed up to a yearly overall Cod Index.

Table 3.2: The choice of stations describing radiation levels within each spawning area.

Area	Stations		
A + B	Vigra	Svinøy	Skrova
C	Skrova	Andøya	
D	Andøya	Hekkingen	Torsvåg
E + F	Torsvåg		

3.5 Effect on total cod stock

There are different ways of quantifying the Arcto-Norwegian cod stock. For this study the year class strength of Arcto-Norwegian cod is used. Year class strength is the number of Arcto-Norwegian cod at the age of three years. The year class data are provided by Svein Sundby and are posted in Table 3.3, along with the mean sea temperature for March and April at 0-50 meters depth at the main spawning area for cod in Lofoten (area C). As the sea temperature mean has variations on a large scale (Gill, 1982) it is believed to be representative for all the spawning areas. Also, the Lofoten area is strongest weighted for all years (see Table 3.1). Year class and sea temperature are also illustrated in Figures 3.9 and 3.10.

Year class data only exist for until 2002, the final Cod Index will therefore only contain data from 1957-2002. It is also worth mentioning that as the calculation of year class strength includes the "counting" of 4th, 5th and 6th year cod as well, the numbers for 2000, 2001 and 2002 may change a bit when new countings are available. This is however, not expected to give a large change in the outcome of this study.

Table 3.3: Mean sea temperature for March and April (0-50 meters depth) for the Lofoten spawning area (area C; see Figure 3.1) and year class strength (in millions).

Year	T° C	Year Class	**Year**	T°C	Year Class
1957	3.166	789	**1982**	2.241	523
1958	2.544	916	**1983**	4.100	1037
1959	3.830	728	**1984**	3.220	286
1960	4.121	472	**1985**	2.621	204
1961	3.592	338	**1986**	2.366	173
1962	2.921	777	**1987**	2.378	242
1963	2.814	1582	**1988**	2.957	412
1964	3.869	1295	**1989**	3.958	721
1965	3.639	164	**1990**	4.097	896
1966	1.725	112	**1991**	3.731	810
1967	2.774	197	**1992**	4.429	659
1968	2.723	404	**1993**	3.570	439
1969	2.488	1015	**1994**	3.309	719
1970	3.395	1819	**1995**	3.411	843
1971	2.292	523	**1996**	2.953	568
1972	3.694	621	**1997**	3.047	623
1973	3.446	613	**1998**	3.527	545
1974	3.234	348	**1999**	3.410	429
1975	3.582	638	**2000**	4.018	546
1976	3.364	198	**2001**	3.412	296
1977	3.333	137	**2002**	3.613	576
1978	2.638	150	**2003**	3.453	
1979	2.326	151	**2004**	3.698	
1980	2.658	166	**2005**	4.046	
1981	1.439	397			

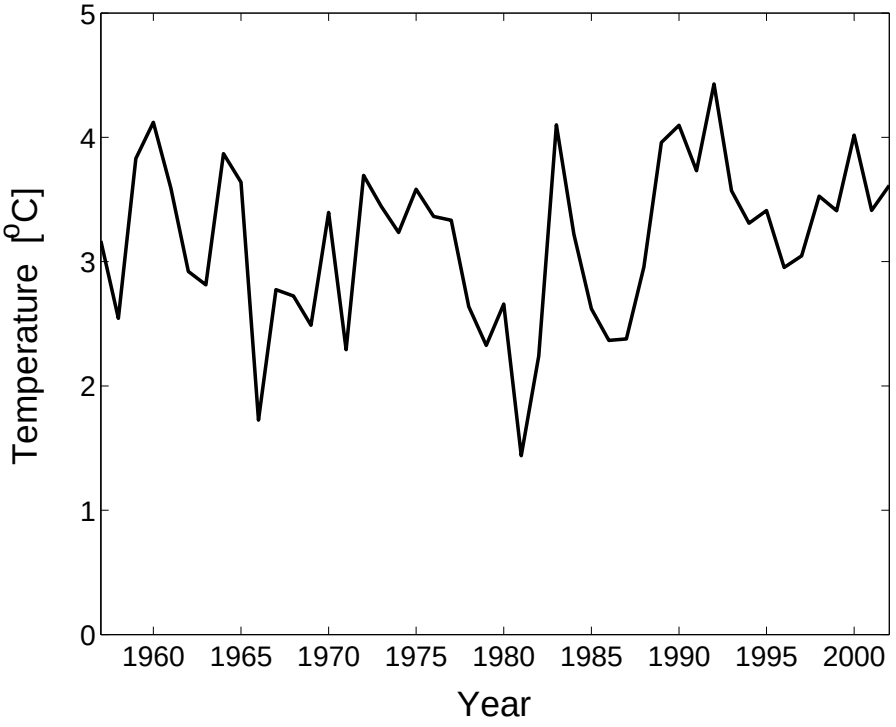

Figure 3.9: Mean sea temperature for March and April, 0-50 meters depth, at the main spawning area for cod in Lofoten (spawning area C from Figure 3.1)

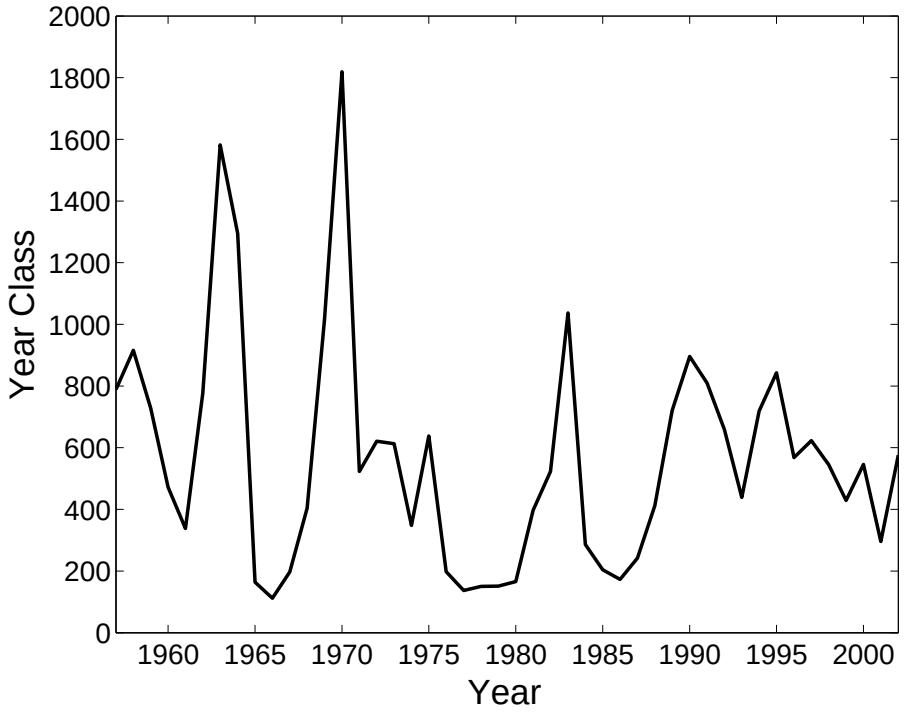

Figure 3.10: Year class strengths (as in number of fish at the age of three years; in million) of Arcto-Norwegian cod.

Chapter 4

Reconstruction of UV radiation

In this chapter the model used for this study is presented, along with a thorough description of the input parameters and the necessary processing of input data.

4.1 STAR

Observed UV radiation is, as described in the introduction, not available for the chosen areas within the current time period. It is therefore necessary to reconstruct UV radiation for the different stations. The modelling of UV radiation requires a radiation transfer model and reliable input data sets.

The model used here, System for Transfer of Atmospheric Radiation (from now on referred to as STAR) is based on the matrix operator code of Nakajima and Tanaka (1986) which solves the radiation transfer equation by using the discrete ordinate and adding method. The model includes databases for atmospheric constituents and considers both absorption and scattering by all UV relevant atmospheric constituents, as aerosol, air molecules, ozone concentration etc. (Reuder and Koepke, 2005).

STAR is developed to estimate surface UV-radiation (UV-A and UV-B), but also includes calculations for radiation in the visible area. In total STAR calculates spectral irradiance in the range from 280 nm to 700 nm, which can be integrated using arbitrary biological weighting functions. STAR was developed for the purpose of scientific use within the topic of UV radiation and its impact on humans, animals and plants, and is free for non-commercial use (Schwander et al., 2001).

STAR comes in two versions, STARsci (Ruggaber et al., 1994) and STARneuro (Schwander et al., 2002). STARsci solves the radiation transfer equation for a cloud free atmosphere or atmosphere with homogenous cloud layers. STARneuro enables the treatment of the atmosphere under realistic cloud conditions. The model used for this work is STARneuro. To describe the multi-layered atmosphere STAR uses variable data sets which contain information of the vertical profile of the atmosphere. The radiative-transfer calculations are made on the basis of atmospheric transmittances which can be characterized by a cloud modification factor (CMF).

$$CMF = E_{cloud}/E_{clear} \quad (4.1)$$

where E_{cloud} is the global irradiance in the presence of clouds and E_{clear} is the global irradiance under the same atmospheric conditions but without clouds (Schwander et al., 2002). The CMF is spectrally dependent, and the dependency is determined on the basis of a neural network algorithm. The neural network is trained under natural conditions in Garmisch Partenkirchen, Germany (Schwander et al., 2002) with cloud observations, AOD, and the position of the sun as variable inputs. With the help of the neural network STAR provides spectrally resolved and weighted irradiance under conditions described by the input data. STAR offers different cloud neural networks to make the most of the available input data, even if cloud data are very limited or if more information, as global radiation is included as well.

To considerably reduce the computational time, STAR only calculates radiation quantities for seven wavelengths in the range 290-610 nm and uses a second neural network to replenish the transmittance spectra to a higher spectral resolution.

For this study both amount and type for low, medium and high level clouds are used as input data. STAR will provide instantaneous values of integrated UV irradiances in Wm^{-2} which have to be multiplied by 3600 s to obtain hourly dose values in Jm^{-2}. If the quality of the data describing the atmospheric constituents is good and the spatial and temporal resolution is high, the output data are expected to be of high quality. STAR has been used for many studies and the results have been of a satisfactory high quality (dependent on the quality of the input parameters) (Reuder and Koepke, 2005; Sætre, 2006). However, a recently published study indicates that the model in many cases overestimates UV radiation, especially for other geographical locations than where the neural network was trained (Koepke et al., 2006).

4.2 Input data STAR

The primary challenge of the modelling operation is to achieve satisfactory quality of the input data. STAR models instantaneous values with a resolution of one hour, so hourly values of the chosen input parameters are needed. Some are obtained by geometrical calculations, while others are fixed, based on previous studies. For the remaining parameters, meteorological observation data (SYNOP) have been an important source of information, along with ozone observations. Data achieved from observing are however characterized by the potential of human and technical errors. The latter limits the continuity, therefore some assumptions and approaches must be made to complete the data sets.

4.2.1 Clouds and other meteorological parameters

As the cloud effect on UV radiation varies according to the characteristic of the different types of cloud scenarios (Chapter 2.2.3), correct and detailed information about

the local cloud conditions corresponding to the areas of interest is crucial for the quality of the UV-modelling. This information should idealistically contain a quantitative description of the amount and type of clouds in the three cloud levels.

As mentioned in Chapter 3.1, six coastal SYNOP stations are found relevant according to the geographical area of interest (Figure 3.1) and the need for a description of the state of the sky. Met.no's SYNOP data were made available for non-commercial initiative at an internet based climate database in 2003 and all available data for these stations are downloaded from there (www.eklima.no). The existence of relevant data is however not a matter of course. Some of the stations are only automatic stations, which means that descriptive observations of cloud conditions are not present. Also, some stations have only been operative for a limited time period or stations have been out of operation because of maintenance or instrumental failure.

Exact location and periods with missing data for the six stations Svinøy, Vigra, Skrova, Hekkingen, Torsvåg and Andøya are summed up in Table 4.1 and Table 4.2.

Table 4.1: Synoptic stations used for UV reconstruction. Andenes was operational until March 1972, but only data from 1957 are used to complete the Andøya data set. All the station information is collected at www.eklima.no.

Station		**Lat**	**Long**	**Period**
87100	Andenes	69.32°N	16.12°E	01.01.1957-1958
87110	Andøya	69.30°N	16.15°E	01.01.1958-2005
88690	Hekkingen	69.60°N	17.84°W	01.11.1979-2005
85380	Skrova	68.15°N	14.65°E	01.01.1957-2005
59800	Svinøy	62.33°N	5.27°E	01.01.1957-2005
90800	Torsvåg	70.25°N	19.50°E	01.01.1957-2005
60990	Vigra	62.56°N	6.12°E	01.07.1958-2005

Processing SYNOP data

Relevant observations include: the pressure at station level, the type of low (CL), middle (CM) and high clouds(CH), the corresponding level of cloud basis, the cloud cover of the lowest cloud layer (CL and CM) (NH), total cloud cover (NN), and additionally all available wind observations which were discussed in Chapter 3.4.3. Preferably the database will provide homogeneous series with hourly observations. But some of the

Table 4.2: Periods with missing cloud observation data. These periods are removed from further calculations. Hekkingen is however, the only station with data missing in spawning months, so the Cod Index is complete for the periods indicated in Table 4.1 above for all stations but Hekkingen.

Station	**Periods**		
Hekkingen	Mar 2004	May 2004-Dec 2005	
Skrova	Aug-Sep 2005		
Svinøy	Aug-Des 2005		
Torsvåg	Oct-Nov 2003	Jan 2004	Sep-Oct 2005
Vigra	Aug-Sep 2005		

series, especially the eldest, only have observations for every 6th hours and for some periods parameters are missing. Days with no or very inadequate cloud observations will be eliminated for further use. The days and periods excluded from further calculations are displayed in Table 4.2. The processing to make the data continuous and readable for STAR is done using Matlab. Firstly the data sets are extended to a temporal resolution of one hour. Secondly, hours where data are missing are filled by data from the last observation hour.

To include Rayleigh scattering as a parameter in the model, pressure information is needed. As only two stations have continuous pressure measurements, pressure at the four remaining stations is characterized by the standardized pressure at sea level (1013.25 hPa). But, most comprehensive of the missing data is the lack of information on cloud amount for the different layers (NCL, NCM, NCH). Typical cloud observations have no additional information about the cloud amount other than NH and NN. To fill out this gap a formulae is deduced which exploits the information already known (NH and NN). The formulae takes the maximum and minimum possible cloud amount into consideration and the outcome is an average of the possibilities.

For weather conditions with poor visibility, like heavy snow-fall or dense fog, the person observing is not able to observe the actual cloud type. This is coded as -3 in the total cloud cover column, with no additional information. A code like this is not readable in STAR, but as both heavy snow fall and dense fog cause considerable attenuation of radiation (Koepke et al., 2002), replacing the code with thick clouds in the lower layer will be a reasonable assumption. To separate fog and snow-fall incidents the year is divided into two seasons; winter and summer. The periods vary with latitude, where the winter season in the south is set to November - March, while winter in the north is

October-April. Every heavy snow-fall incident is placed in the winter season and the dense fog in the summer season. Snow incidents are coded with 8/8 of Cumulonimbus (Cb) in the lower layer, while fog incidents are coded to 8/8 of Stratus clouds in the lower layer, both incidents with a cloud basis elevation of zero meters.

The SYNOP data from met.no are archived with codes according to met.no‘s own weather codes. This includes unique codes for the specific type of clouds in each of the three cloud layers (low, middle, high) and with the cloud amount measured in oktas, where zero is a clear sky condition and eight overcast. STAR operates with another system, so all the codes from met.no are transformed. This transformation is almost straight forward, but as STAR uses fewer cloud types at the different levels and the definitions for certain cloud types are different, some cloud types are redefined or moved to an other level. The conversion of codes is shown below in Table 4.3.

Table 4.3: Transformation of met.no SYNOP cloud codes to STAR cloud codes. Low clouds: Cumulus (Cu), Cumulonimbus (Cb), Stratocumulus (Sc), Stratus (St), Nimbostratus (Ns). Middle clouds: Altostratus (As), Nimbostratus (Ns) Altocumulus (Ac). High clouds: Cirrus (Ci), Cirrostratus (Cs), Cirrocumulus (Cc).

a)										
Low clouds	Cu	Cu	Cb	Sc	Sc	St	St	Cu	Cb	Ns
met.no	1	2	3	4	5	6	7	8	9	**X**
STAR	4	4	5	2	2	1	1	4	5	3
b)										
Middle clouds	As	Ns	Ac	Ac	Ac	Ac	Ac	Ac	Ac	
met.no	1	2	3	4	5	6	7	8	9	
STAR	2	**X**	1	1	1	1	1	1	1	
c)										
High clouds	Ci	Ci	Ci	Ci	Cs	Cs	Cs	Cs	Cc	
met.no	1	2	3	4	5	6	7	8	9	
STAR	1	1	1	1	2	2	2	2	2	

4.2.2 Ozone

The time period of interest is a rather bold choice when looking at the fact that there are exclusively few stations world wide with a long enough history of ozone measurements. Stations in Norway meeting this demand are even fewer in number. But Tromsø, with one of the longest total ozone records in the world with measurements dating back to 1935, will provide most of the ozone data needed (Svenøe, 2000). As variations in the ozone is mainly a large scale process, the Tromsø data are assumed representative for all stations within the Lofoten area. This assumption is supported by Lindfors et al. (2003) which found good agreement between ozone measurements at Tromsø and Sodankylä, 400 km apart.

For the current time period the Tromsø data provide almost a continuous data set consisting of observations from a Dobson spectrophotometer. The data are assumed to hold a high quality (Svenøe, 2000). It operates on the simple principle of how ozone absorption of UV radiation strongly depends on wavelength, where UV radiation with short wavelengths are heavily absorbed by ozone and UV radiation with longer wavelength is nearly unaffected by ozone. Unfortunately the Dobson spectrophotmeter in Tromsø was temporarily out of order due to a technical failure in late spring 1972 and the measurements were absent until November 1984. After this it ran until end of 2001, from the mid 1990s with a Brewer instrument operating parallel (Svenøe 2000). The Brewer data are only used if Dobson data are not present (Svenøe, 2000).

The Tromsø Dobson, Brewer and TOMS (Total Ozone Mapping Spectrophotmeter) data are most gratefully provided by Georg Hansen at the Norwegian Institute for Air Research (NILU). TOMS data are satellite based ozone observations and differences between ground observations of ozone and TOMS are known to exist (Fioletov et al., 1999). Carlson (2005) for example shows systematically higher ozone observations from TOMS than ground based measurements for many cases. This overestimation is suggested to be caused by tropospheric aerosols (Chipperfield and Fioletov, 2007). TOMS data are therefore not preferred, this is however, the only data available for the time period 1979-1985, so it is used here.

Despite of now having three different data types of ozone observations the ozone data set is not complete for the time period 1973-1979. To fill this gap a monthly decadal (1966-1975, 1976-1985) average is calculated. To fill the four missing years in the end of the period, 2002-2005, Brewer data from Andøya, also provided by Georg Hansen, are used. The Brewer data roughly contain ozone measurements from only March until mid October. The sun is completely absent in the Lofoten area from late November until late January so the ozone amount for this period will make a negligible influence on the UV radiation. The total ozone amount for these days are therefore set to a standard value of 300 DU. The remaining days with missing data are days when the sun is close to the horizon. For low solar elevations measures of the radiation itself give large uncertainties (Olseth and Skartveit, 1993). It is therefore reasonable to expect large uncertainties in the ozone-measurements at these times as well, and thus not unreasonable to use a decadal (1996-2005) monthly mean for these days as well.

In contrast to the long ozone data set at Tromsø, there are no ozone measurements from stations within a reasonable range of the stations west of Møre, Vigra and Svinøy. To obtain a continuous ozone data set here all available ozone observations within the coordinates 10° west to 40° east and 55° to 80° north from the database WOUDC (World Ozone and Ultraviolet Radiation Data Center) are collected. WOUDC provides ozone data from 20 stations within the selected range. The data are interpolated with the Cressman interpolation, an interpolation routine where the ozone data from the different stations are weighted as a function of distance between the ozone station and the target point (http://ingrid.ldeo.columbia.edu/dochelp/StatTutorial/Interpolation/, 2007). The existence of ozone data from the 20 different stations is very variable. But for most stations the data sets only contain measurements for a few years, the Tromsø data set is therefore very dominant in the interpolation.

4.2.3 Solar elevation

Solar elevation in STAR simulations is defined by latitude and longitude of the location, and time and date. At areas between 62° - 70° north the solar elevation varies annually with one maximum and one minimum when the sun is at its greatest distance from the equator plane. Lofoten is located north of the polar circle and in the weeks around the summer solstice (around 23th of June) the area experiences midnight sun (around 19th of May to 23th of July). In the winter the opposite happens with polar night (around 23th of November to 13th of January) in the weeks before and after the winter solstice (around 21st of December) (met.no, 2007). During these special events the UV radiation is expected to reach a maximum and minimum. The areas around Vigra and Svinøy are located south of the polar circle and have no midnight sun nor polar night, but because of the sub-polar location there are many sun hours in summer and few in winter.

4.2.4 Turbidity

The turbidity of the atmosphere is the main factor determining scattering and/or absorption of radiation by aerosols. As described in Chapter 2.2.4 the turbidity of the air is determined by the aerosol content, its chemical composition (i.e. aerosol type), its vertical distribution and the corresponding humidity profile. Actual aerosol information is not available for the period and locations of UV reconstruction. Therefore, reasonable assumptions have to be applied.

STAR provides several typical aerosol types, e.g. maritime clean (mc), maritime polluted (mp), continental clean (cc), continental average (ca) and urban (ur). Since all the stations in this study are coastal stations with onshore winds dominating, the aerosol type maritime clean has been selected. The optical depth is known to vary through the seasons (see Chapter 2.2.4). For the UV reconstruction, the optical depth is set according to literature values (Olseth and Skartveit, 1989) to 0.1 in winter (December-February), 0.15 in spring and autumn (March-May and September-November) and finally 0.2 in summer (June-August). The humidity profile that affects the turbidity

by potential swelling of the aerosol particles, is prescribed as seasonal average for mid-latitudes.

4.2.5 Albedo

As mentioned in Chapter 2.2.5, the majority of natural surfaces has an albedo lower than 0.1. Sea and vegetation covered land surfaces can be described by a constant albedo of 0.03 (Koepke et al., 2002). Even though the presence of snow cover in a several kilometer radius around the observer is known to increase UV irradiance (Kerr and Seckmeyer, 2003), snow is not considered in this study because of incompleteness of snow data for these locations. This decision is however defendable by the fact that the spawning areas are near the coast, with some distance from snow covered surfaces potentially influencing the UV radiation at the spawning areas.

Chapter 5

Results and Discussion

In the first part of the chapter an assessment of the modelled data is presented through a comparison between modelled data and observed ground UV (GUV). Yearly and seasonal plots are shown, in addition to statistical means with a following discussion of the quality of the model data. Secondly trends in the reconstructed UV radiation are presented and the mechanisms behind discussed. The second part of this chapter starts with a presentation of the result for each component of the Cod Index, followed by a description of the Cod Index and the trends and variability at each station. Finally the overall Cod Index is presented with a discussion of the possibility of a connection with the year class data.

5.1 Comparison of STAR-UV and GUV

5.1.1 Measured UV data

Erythemal weighted UV irradiance has been measured at Andøya by the Norwegian Radiation Protection Authority (NRPA) since 2000 with instrumentation located on top of a 380 meter high mountain (see http://alomar.rocketrange.no/guv.html (2007) for more information). The irradiance is measured with a time resolution of one minute, but the data used for this study is one hour averages and has been provided by Bjørn Johnsen at NRPA.

As STAR has been used to estimate hourly erythemal UV for Andøya comparison between these two quantities will give indications on the quality of the modelled values. It is however, important to keep in mind that even the best measurements of UV_{ery} have a total accuracy of $\pm$ 10 % (personal correspondence, Bjørn Johnsen). Observations from the period 2000-2004 have been included in the following comparison.

5.1.2 Modelled vs Observed UV radiation

The comparison is presented as daily and hourly values for each year (2000-2004) in Figures 5.1 and 5.2, respectively. Besides, the seasonal (winter, spring, summer and autumn) variation of hourly and daily values of four of the years (2000-2003), is also

presented in Figures 5.3 and 5.4, respectively. In addition, the corresponding statistical quantities are given in Tables 5.1-5.4.

To exclude potential error during nighttime, observed values between sunset and sunrise are set to zero. Hours and days with missing observations are excluded from the comparison. The number of observation and modelled hours to be compared is in total 20787.

Table 5.1: Correlation coefficient (R^2), Root-Mean-Square deviation (RMSD) and mean bias deviation (MBD) of the modelled daily UV doses compared to measurements corresponding to the plots presented in Figure 5.1. N is number of days. RMSD and MBD are both shown in Jm^{-2} and %.

Year	R^2	RMSD	MBD	N
2000-04	0.94	307(37%)	-69(-8%)	1420
2000-03	0.96	259(30%)	-71(-8%)	1109
2000	0.94	274(30%)	-43(-5%)	251
2001	0.95	271(33%)	-65(-8%)	251
2002	0.97	256(31%)	-91(-11%)	309
2003	0.97	236(29%)	-81(-10%)	298
2004	0.86	438(55%)	-61(-8%)	311

Table 5.2: Correlation coefficient (R^2), Root-Mean-Square deviation (RMSD) and Mean Bias Deviation (MBD) of the modelled hourly UV doses compared to measurements corresponding to the plots presented in Figure 5.2. N is number of hours. RMSD and MBD are both shown in Jm^{-2} and %.

Year	R^2	RMSD	MBD	N
2000-04	0.90	33(57%)	-5(-8%)	20787
2000-03	0.92	29(51%)	-5(-8%)	16360
2000	0.87	31(53%)	-3(-5%)	3904
2001	0.92	29(52%)	-4.4(-8%)	3737
2002	0.93	29(50%)	-6(-11%)	4386
2003	0.93	28(49%)	-6(-10%)	4333
2004	0.82	43(77%)	-4.3(-8%)	4427

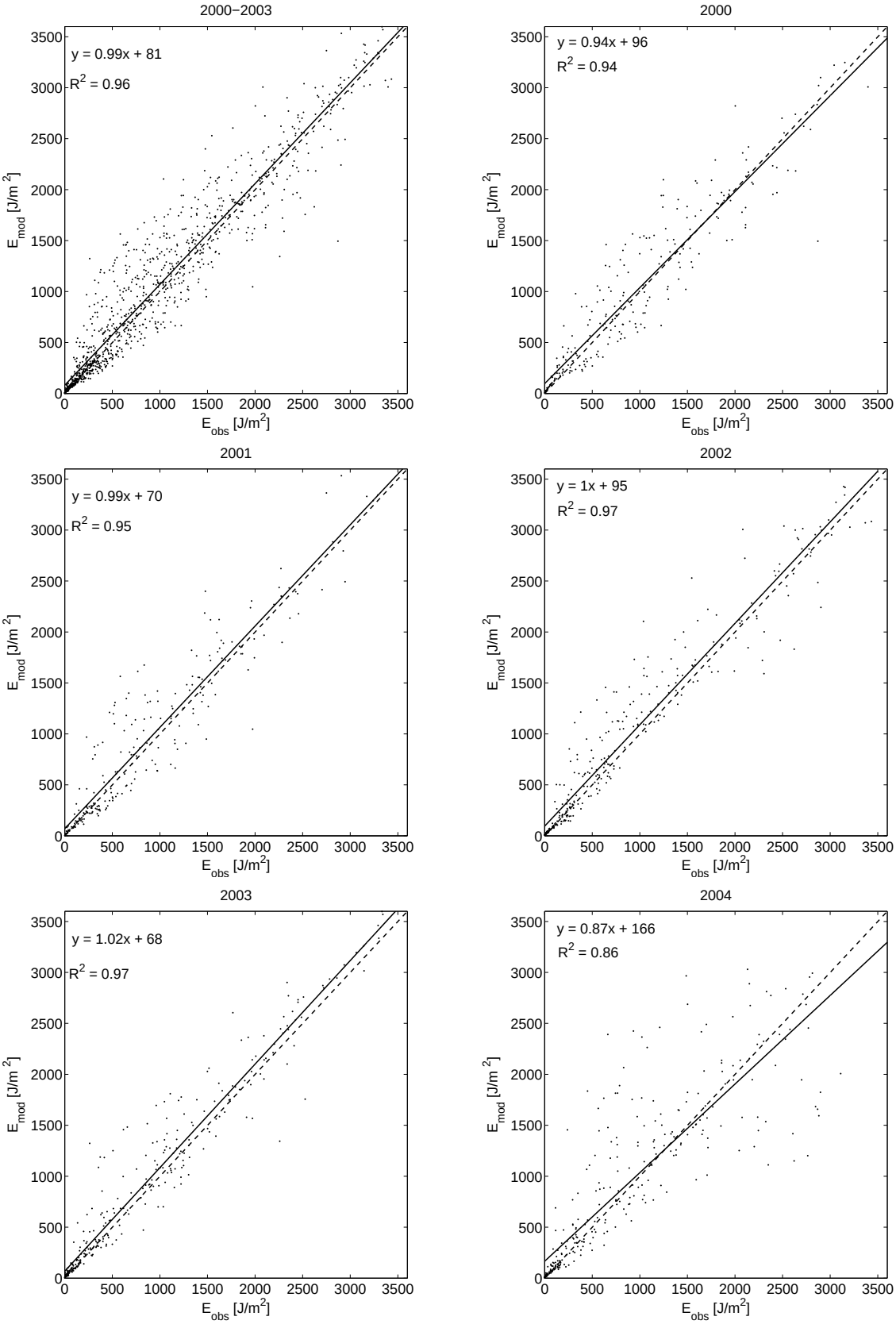

Figure 5.1: Modelled versus observed daily erythemal UV doses at Andøya for each of the years 2000-2004, and for the period 2000-2003 collectively (see text). Also shown: The one-to-one line (broken), regression line (solid) with corresponding equation and the correlation coefficient R^2.

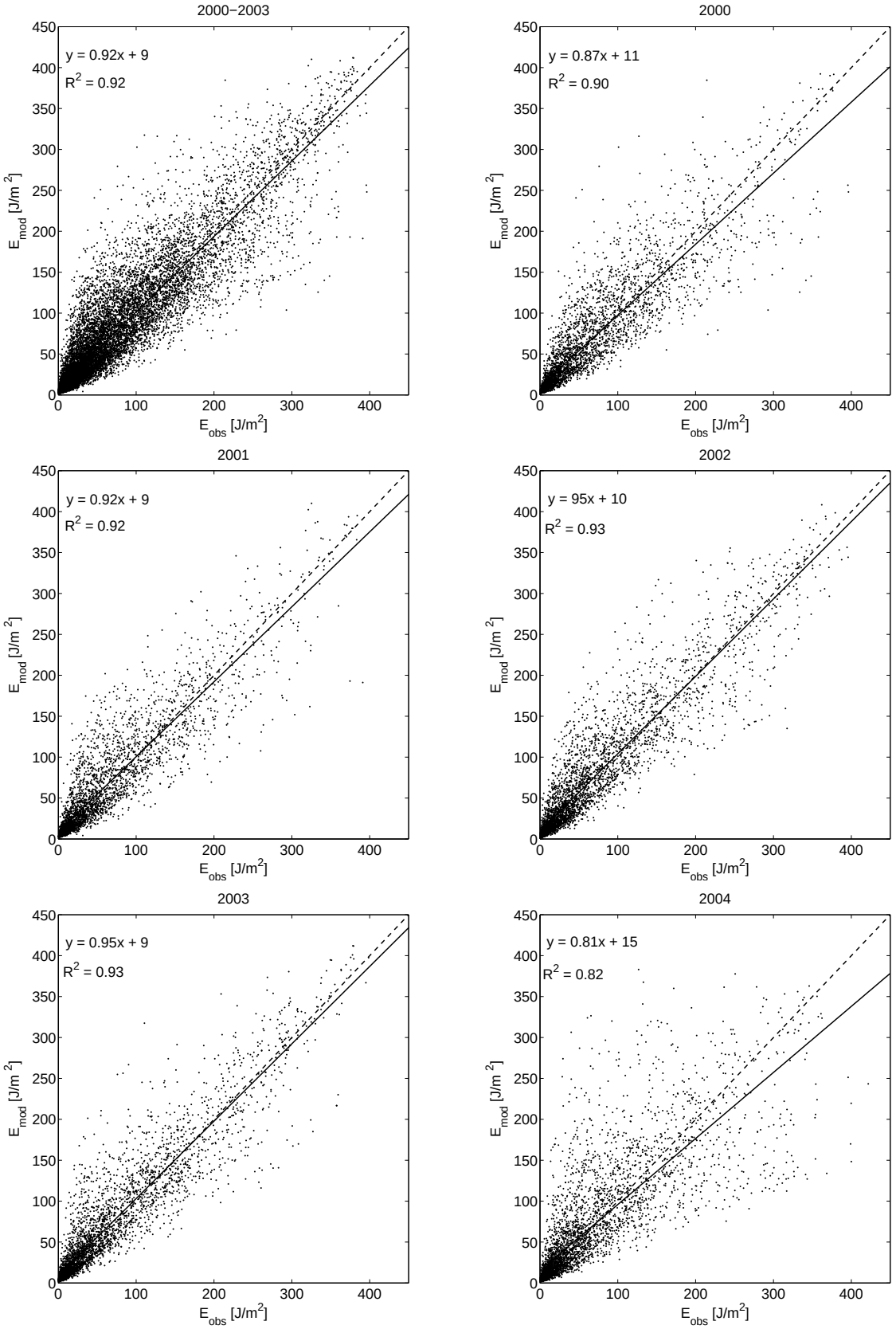

Figure 5.2: Modelled versus observed hourly erythemal UV doses at Andøya for each of the years 2000-2004, and for the period 2000-2003 collectively (see text). Also shown: The one-to-one line (broken), regression line (solid) with corresponding equation and the correlation coefficient R^2.

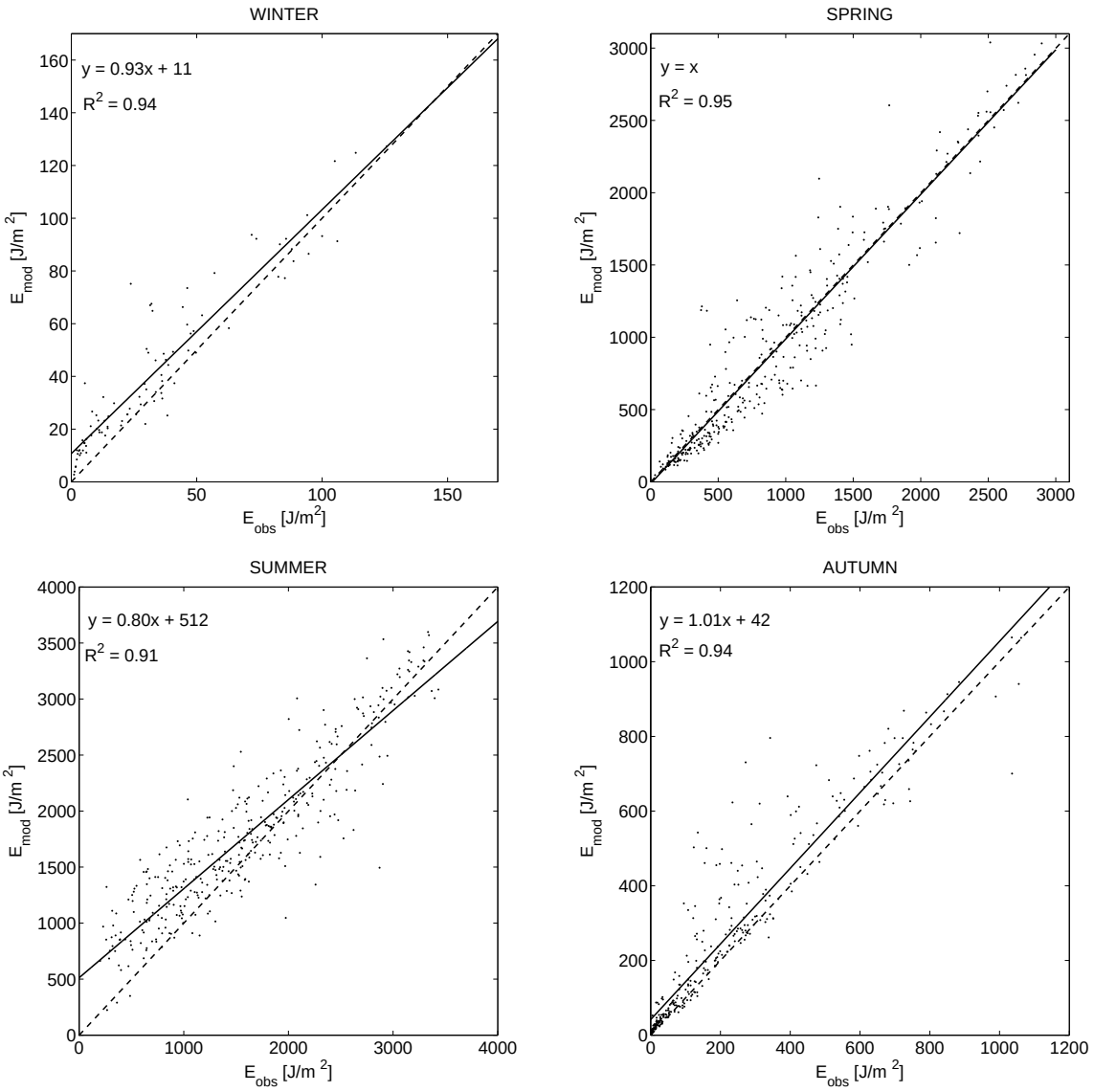

Figure 5.3: Modelled versus observed daily erythemal UV doses at Andøya. Winter: Jan-Feb, Spring: Mar-May, Summer: Jun-Aug, Autumn: Sep-Nov 2000-2003. Also shown: The one-to-one line (broken), regression line (solid) with corresponding equation and the correlation coefficient R^2.

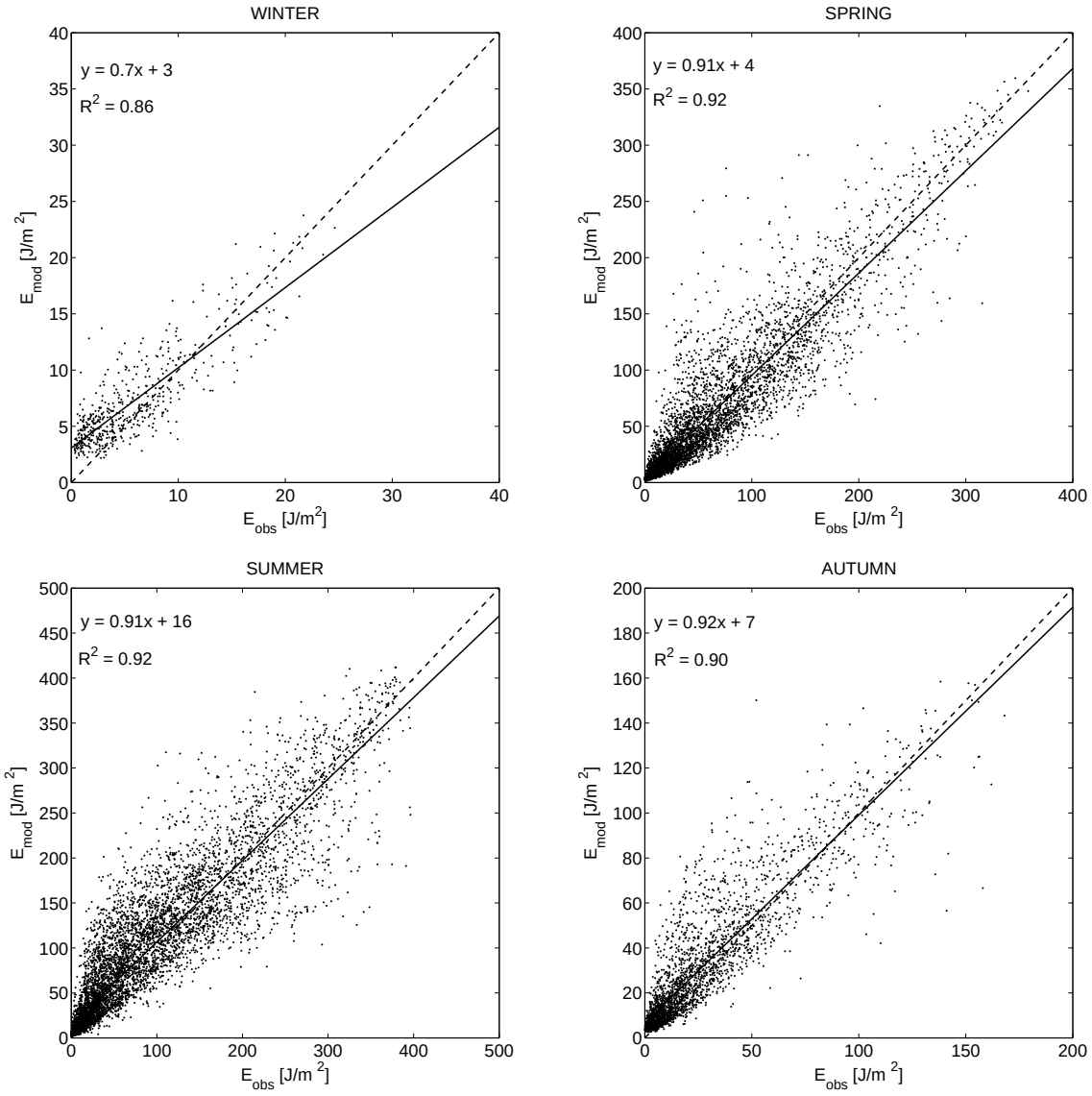

Figure 5.4: Modelled versus observed hourly erythemal UV doses at Andøya 2000-2003. Winter: Jan-Feb, Spring: Mar-May, Summer: Jun-Aug, Autumn: Sep-Nov. Also shown: The one-to-one line (broken), regression line (solid) with corresponding equation and the correlation coefficient R^2.

Table 5.3: Correlation coefficient (R^2), Root-Mean-Square deviation (RMSD) and Mean Bias Deviation (MBD) of the modelled daily UV doses compared to measurements corresponding to the plots presented in Figure 5.3. N is number of days. RMSD and MBD are both shown in Jm^{-2} and %.

Season	R^2	RMSD	MBD	N
Winter	0.94	13(39%)	-8(-24%)	90
Spring	0.95	218(24%)	12(+1%)	337
Summer	0.91	392(25%)	-190(-12%)	360
Autumn	0.94	96(45%)	-44(-21%)	322

Table 5.4: Correlation coefficient (R^2), Root-Mean-Square deviation (RMSD) and Mean Bias Deviation (MBD) of the modelled hourly UV doses compared to measurements to the plots presented in Figure 5.4. N is number of hours. RMSD and MBD are both shown in Jm^{-2} and %.

Season	R^2	RMSD	MBD	N
Winter	0.86	3(50%)	-1(-24%)	527
Spring	0.92	25(44%)	1(+1%)	5337
Summer	0.92	37(49%)	-9(-12%)	7588
Autumn	0.90	14(58%)	-5(-21%)	2908

The general agreement of the comparison between modelled and observed daily values at Andøya in Figure 5.1 is good, but a certain spread is present. The correlation coefficient for the individual years (2000-2003) shown in Table 5.1 lies within the range of 0.94-0.97 with a RMS deviation of around 30 %. The corresponding means for the whole period are R^2= 0.96 and RMS deviation = 30 %. The high RMS deviation was expected, as no information of global radiation is included in the modelling. Without global radiation there is a large uncertainty of the exact position of the clouds relative to the sun when a broken cloud cover is present. In Koepke et al. (2006) UV irradiances are modelled by STAR with global radiation as input, and the spread is automatically much less.

The RMS deviation for 2004 (55 %) is considerably higher as shown in Figure 5.1 and Table 5.1, the correlation coefficient of 0.86 is also much lower than for the other

years. Personal correspondence with Bjørn Johnsen, who is responsible for the instrumentation at NRPA, revealed that parts of the observations from 2004 are presumably incorrect because of a leakage on the instrumentation. Observations from 2004 are therefore left out in the plot of the total period, but is placed in the overview of individual years to illustrate the outcome of an instrumentational error. 2000 also stands out with a smaller correlation coefficient, but the RMS deviation is average. The low correlation could be due to a limitation in the SYNOP cloud observation which were only available for every 3rd hour this year. This causes additional uncertainty in the cloud description used as model input.

The slope of the regression lines of the individual years in Figure 5.1 shows values from 0.94-1.02 with intersection with the y-axis at 68-96. The corresponding numbers for the whole period (2000-2003) are a slope of 0.99 and an intersection at y = 81. The limitations in cloud observations in 2000 result in a lower value of the slope (94) but the intersection with the y-axis is a little bit higher than the remaining years (2001-2003). The year 2004, however, clearly reflects the instrumentational problems as the slope of the regression line is 0.87 with an intersection of 166.

There seems to be a slight overestimation for modelled values, especially for low UV radiation. The overestimation can be identified by looking at the intersection of the regression line with the y-axis, also the mean bias deviation in Table 5.1 is negative. The potential reasons for the overestimation of low UV values are many. Sætre (2006) pointed out that STARneuro is trained for a continental environment in southern Germany. Systematic differences in microphysics (e.g. droplet size distribution and average water liquid content) and macrophysical (e.g. average geometric thickness of the clouds) cloud properties will result in discrepancies. It is also mentioned by Sætre (2006) that the model could underestimate enhanced absorption within clouds (see Chapter 2.2.3).

The correlation coefficient for hourly plots shown in Table 5.2 are in the range 0.87-0.93, which is smaller than for the daily plots. The RMS deviation is also considerably higher, with values of 49-53 %, hence a bigger spread is present here than for daily plots. As previously mentioned the spread is mainly because of the lack of global radiation information bringing uncertainties of the position of the sun for a broken cloud cover. But also, the model only provides an instantaneous value once every hour which is multiplied by 3600 to achieve hourly values (Chapter 4.1), while observed values are observations taken every minute summed to hourly values. I.e. any variability in the state of the cloud between hours are left out in modelled values, but included in observed values. For daily values the RMS deviation related to these two problems is somewhat evened out, but for hourly values the uncertainty is manifested in every single observation. The erroneous data measurement from 2004 and the lack of hourly cloud information for 2000 can also be identified in the hourly plots.

The comparison of modelled and observed values according to season in Figures 5.3 and 5.4 enables an extra focus on data used for calculation of the Cod Index. Worth mentioning for seasonal plots is that late autumn, winter and early spring days bring

the potential of snow cover on the surrounding ground. As snow is not accounted for in the model, this could lead to an underestimation of UV doses by the model.

The daily plots show correlation coefficients in the range 0.91-0.95 with a RMS deviation of 24-45 % (Table 5.3). The lowest correlation coefficient is for the summer season. In most of summer Andøya experiences midnight sun (see Chapter 4.2.3) but the model clearly overestimates for low daily summer values. One explanation could be due to underestimation of the influence of the clouds when the sun is high and thick clouds are present. The regression lines show that the relative deviation is largest for low GUV values for summer and winter plots. So an overestimation obviously occur also in winter. It is however, not uncommon that a model fails to generate sufficient low values for extreme cases like a low winter sun. The relative error can easily grow large at this time of the year and the percentage Root-Mean Square increases.

Other potential sources of errors mainly for winter plots, is a potential underestimation of the model due to the lack of snow information as mentioned above. Also, many of the days between November and February do not have ozone measurements, and a decadal average was used instead (Chapter 4.2.2). Even with an uncertainty of only ± 2.5 % in the ozone data, the UV irradiance can be considerably higher or lower, especially for high solar zenith angles (low sun as often in winter and late autumn) (Schwander et al., 1997). The problems in winter and summer however are not a further issue in this work, because the calculations of the Cod Index use spring time doses only. For this season the slope of the regression line of the daily plot is one and can be considered an excellent agreement between reconstruction and measurement.

The seasonal plots of hourly values shown in Figure 5.4 have a correlation coefficient within the range 0.86-0.92 (Table 5.4). As for daily plots winter shows the smallest correlation coefficient with 0.86, where again the main feature seems to be an overestimation of low values. A relatively large spread, characteristic of modelling without data on global radiation, is present in all plots, but spring values have the smallest RMS deviation and the mean error is merely present.

With an excellent agreement between reconstructed and measured daily values for spring and a relatively good agreement for hourly values the reconstructed UV radiation used for calculating the Cod Index is considered to be well representative.

5.2 Trends in UV radiation

The modelling of UV radiation for the spawning areas has provided a continuous data set of UV-A, UV-B and cod weighted radiation for 49 years. Positive trends in UV radiation have been observed and calculated for several places during the last couple of decades (e.g. Häder et al. (2007)), and it will be interesting to look for similar trends in the reconstructed UV for the spawning areas.

Decadal monthly trends for UV-B, UV-A and cod radiation (CodUVB and CodUVAB) for the time period with existing input data are shown in Tables 5.5- 5.10. The reconstruction for Hekkingen covers only the period 1980-2003, for Vigra mainly for 1959-2005. Years with missing data for the four remaining stations are also excluded (see Table 4.2 for details) from the trends. The tables also show trends of ozone (O_3) corresponding to the period of UV radiation reconstruction.

UV-B radiation at the surface for a fixed solar elevation is determined by both cloud and ozone, while UV-A radiation is predominantly affected by clouds (Chapter 2.2.2 and 2.2.3). Therefore the trends in UV-A radiations will reflect changes in cloud extinction, by changes in cloud amount and/or a change towards more opaque cloud.

Mainly UV-B and UV-A radiation will be discussed in the following. Trends in cod weighted radiation are expected to appear similar to the trends in UV radiation, according to the weighting spectrum in Figure 3.3. Spring months will be emphasized, as this is the time of the spawning.

5.2.1 Southern stations, 62.33-62.56 ^{o}N

Svinøy and Vigra

As seen in Table 5.5 and 5.6 the decadal trends at Svinøy and Vigra for UV-A radiation are generally negative throughout the year, where the first three months are most dominating (-1.8 to -3.3 %). This can be explained by an increase in cloud extinction.

For UV-B radiation the decadal trends in Table 5.5 and 5.6 are predominantly positive for the first half of the year. Trends for the second half are less significant and will not be further discussed. The trends are largest (+3.3 to +5.0 %) for March and April which includes 52 of the 62 spawning days. The strong trends correspond to the negative trends in ozone (-1.6 to -2.5 %) but an increase in cloud extinction dampens the effect of the negative trends in ozone on UV-B radiation. The cloud effect can be identified when comparing February and March at Svinøy (Table 5.5) where the negative trend in ozone is similar for both months, but the negative trend in UV-A is stronger in March than in February. Because the cloud extinction is larger in March the trend in UV-B radiation is more dampened here.

5.2.2 Northern stations, 68.15-70.25 ^{o}N

Skrova, Andøya and Torsvåg

Trends in the UV-A radiation are slightly positive throughout the whole year at Torsvåg and Skrova (Tables 5.7 and 5.10). There is a slight positive trend for March-May at Torsvåg (+1.7 to +2.0 %), but rather insignificant for the corresponding months at Skrova (-0.1 to +1.0%). Trends in UV-A radiation at Andøya (Table 5.8) are mostly insignificant (-1.8 to +0.8) throughout the whole year, indicating widely unchanged

average cloud conditions.

For the three northern stations, with data for the period 1957-2005, the decadal trend in UV-B radiation is stronger than at the southern stations and appears positive for most of the year. Again the trends for March and April are most pronounced (+7.2 to +14.2 %), but also May shows positive trends (+2.9 to +5.2 %).

As total ozone content at all the northern stations are given by the Tromsø ozone data set (see Chapter 4.2.2) all spring months have the same negative trend in ozone (-1.5 to -2.8 %). At Torsvåg the positive trend in UV-A radiation, i.e. an decrease in cloud extinction, plus a decrease in ozone explains the increase in UV-B radiation. The trend in UV-A radiation at the remaining two stations are weaker, and the increase in UV-B radiation is only partly dampened.

Hekkingen

As shown in Table 5.9 the trends for Hekkingen are only calculated for the last two and a half decades, and it is interesting to observe the alteration in trends when the time period is changed.

UV-A radiation for Hekkingen shows a positive trend for April, but dominantly negative for the rest of the year. For UV-B radiation there is a strong positive trend for April (+14.5 %), but slightly negative for March and May (-1.6 - -2.3 %), and with varying trends for the remaining months. The strong trend in UV-B in April can be explained by a prominent negative trend in ozone and a parallel increase in UV-A radiation, i.e. a decrease in cloud extinction. For March and May the negative trends in ozone are weak, but a significant negative trend in UV-A indicates a increase in cloud extinction, resulting in a slightly negative trend in UV-B radiation.

5.2.3 General evaluation

As shown in Tables 5.5-5.10 trends in UV-A radiation for spring months are mostly insignificant for Andøya and Skrova (-0.4 - +1.0 %), slightly positive at Torsvåg (+1.7 - +2.0 %), slightly negative for Vigra and Svinøy (-3.3 - -0 %), while at Hekkingen, which has data for half of the period of the other stations, the trends are negative for March and May (-6.7 - -2.8 %) but positive for April (+2.2 %). For UV-B, the trends for corresponding months are mostly positive. This is connected with a general negative trend in ozone for the corresponding months and locations. For some stations the trends are amplified by reduction in cloud extinction given by trends in UV-A radiation mentioned below, or as for Svinøy and Vigra and partly Hekkingen, dampened by higher cloud extinction.

The negative trend in ozone observed for spring months at all six stations seems mainly to be determined by generally lower ozone values in the 1980s and 1990s than before 1980, with several extreme lows in the 1990s. The years 1992 and 1993 were exceptional

because of the effects following the volcanic eruption of Mount Pinatubo in June 1991, where large amounts of aerosols were injected into the stratosphere forming a global layer of sulfuric acid. This led to a substantially increased ozone destruction that was notable world wide (Chipperfield and Fioletov, 2007).

In the Tromsø data set extreme low spring values are also observed for 1996/1997. On a closer inspection relatively low values occur in 1996 for both March and April, while in 97 an exceptional extreme low occur in April. This is probably due to the polar vortex, where chemical reactions between polar stratospheric clouds and CFCs catalyze photochemical destruction of ozone. As Svinøy and Vigra ozone data are interpolated values (Chapter 4.2.2), the influence of the polar vortex is noticeable here as well, even though the phenomenon normally is associated with polar areas.

The Tromsø data show more extreme lows in April than March for the years after mid 1990s, but the ratio between April lows before and after 1980 are lower than the ratio between March lows before and after 1980. This together with the observation of a higher cloud extinction in April and lower in March explains why the negative trend in ozone is strong in April and weaker in March for Hekkingen (Table 5.9, while negative trends are strongest in March for stations with data for 1957-2005 (see Tables 5.5-5.8 and 5.10).

The negative trend in ozone and positive trend in UV-B radiation observed in Tables 5.5-5.10 correspond to studies recently published (Engelsen et al., 2004; Chipperfield and Fioletov, 2007; Fioletov et al., 1999). But as pointed out by literature (e.g. Chipperfield and Fioletov (2007); Fioletov et al. (1999)) and observed in the ozone data set used in this study, the average yearly total column ozone for the Northern Hemisphere has increased slightly after the extreme lows in the 1990s. This is believed to be a direct cause of a decreasing amount of CFCs in the atmosphere, regulated by the Montreal Protocol (Bais and Lubin, 2007).

As April is the month strongest weighted in temporal distribution of the spawning, all stations seem to have experienced an increase in UV-radiation during spawning season. In addition, the strongest trends are observed at the northern stations, which are strongest weighted in the spatial distribution of the spawning. The positive trends in UV-B radiation in Tables 5.5-5.10 are reflected in the cod weighted radiation (CodUVAB and CodUVB) in the corresponding Tables, which also have a significant positive trend during spring. This indicates that there has been an increase in UV radiation in the spectral region with highest cod egg sensitivity.

Table 5.5: Monthly decadal trends at Svinøy 1957-2005, given in %.

Month	CodUVAB	CodUVB	UV-A	UV-B	O_3
January	-0.7	+0.9	-2.9	+1.3	-1.4
February	+1.5	+3.2	-2.2	+5.2	-2.5
March	+ 0.4	+2.6	-3.3	+3.5	-2.5
April	+2.2	+ 3.4	-0.6	+3.3	-1.6
May	+ 0.3	+ 0.7	-0.8	+ 0.7	-1.0
June	-0.9	-0.8	-1.4	-0.8	-0.5
July	-0.9	-0.7	-1.5	-0.7	-0.6
August∗	-1.1	-1.0	-1.4	-1.0	-0.2
September∗	+ 0.8	+ 1.0	+0.1	+0.9	-0.3
October∗	-1.3	-1.4	-1.2	-1.5	+0.3
November∗	-0.8	-0.5	-1.6	-0.6	-0.4
December∗	-1.5	-1.5	-2.2	-1.3	-0.2

Table 5.6: Monthly decadal trends at Vigra 1958-2005, given in %.

Month	CodUVAB	CodUVB	UV-A	UV-B	O_3
January§	+ 0.3	+ 2.1	-1.9	+ 2.1	-1.6
February§	+ 0.8	+ 2.3	-1.8	+ 3.6	-2.0
March§	+ 1.9	+4.3	-2.2	+5.0	-2.4
April§	+ 3.3	+ 4.7	-0.0	+4.6	-1.8
May§	+ 0.7	+ 1.1	-0.4	+1.1	-0.9
June§	+ 0.1	+ 0.3	-0.5	+ 0.2	-0.4
July	-0.2	-0.1	-0.5	-0.1	-0.7
August∗	-0.6	-0.5	-0.8	-0.5	-0.2
September∗	+ 1.8	+ 2.0	+1.2	+1.9	-0.2
October	+0.1	-0.0	-0.0	+0.0	+0.2
November	-0.5	-0.2	-1.1	-0.3	-0.4
December	-0.9	+ 0.8	-1.6	-0.7	-0.4

∗trends only for 1958-2004.
§trends only for 1959-2005.

Table 5.7: Monthly decadal trends at Skrova 1957-2005, given in %.

Month	CodUVAB	CodUVB	UV-A	UV-B	O_3
January	-	-	-	-	-
February	+1.6	+4.2	-1.2	+5.1	-2.1
March	+4.7	+7.5	-0.1	+10.6	-2.8
April	+6.3	+9.4	+1.0	+9.3	-2.3
May	+2.7	+3.7	+0.4	+3.5	-1.5
June	+2.9	+3.3	+1.6	+3.1	-0.8
July	+3.4	+4.1	+1.4	+3.8	-1.5
August$*$	+0.9	+1.1	+0.1	+1.0	-0.5
September$*$	+2.8	+3.5	+1.5	+3.3	-0.7
October	+0.2	+0.1	+0.8	+0.1	+0.5
November	-0.3	-0.8	+0.0	-0.4	+0.2
December	-	-	-	-	-

Table 5.8: Monthly decadal trends at Andøya 1957-2005, given in %.

Month	CodUVAB	CodUVB	UV-A	UV-B	O_3
January	-	-	-	-	-
February	+1.3	+3.6	-1.8	+4.1	-2.1
March	+4.5	+7.1	-0.4	+10.8	-2.8
April	+4.3	+7.0	-0.4	+7.2	-2.3
May	+2.0	+2.9	-0.3	+2.9	-1.5
June	+2.0	+2.5	+0.8	+2.3	-0.8
July	+1.6	+2.3	-0.2	+2.0	-1.5
August	+0.1	+0.3	-0.6	+0.3	-0.8
September	+0.5	+0.9	-0.5	+1.0	-0.7
October	+0.2	-0.4	+0.2	-0.5	+0.5
November	-1.1	-1.5	-0.9	-1.3	+0.2
December	-	-	-	-	-

$*$trends only for 1957-2004.

Table 5.9: Monthly decadal trends at Hekkingen 1980-2003, given in %.

Month	CodUVAB	CodUVB	UV-A	UV-B	O_3
January	-	-	-	-	-
February	-3.6	-6.8	-1.0	-7.1	+3.1
March	-4.5	-1.1	-6.7	-1.6	-0.6
April	+10.7	+14.3	+2.2	+11.4	-3.3
May	-2.5	-2.4	-2.8	-2.3	-0.4
June	3.0	+3.1	+2.1	+3.1	-1.1
July	-2.2	-2.0	-2.5	-2.0	-0.4
August	-5.9	-6.2	-6.0	-5.8	-0.3
September	+0.6	+2.0	-2.0	+2.1	-2.2
October	+6.7	+6.5	+4.2	+9.9	-2.3
November	-2.6	-3.9	-1.1	-4.0	+1
December	-	-	-	-	-

Table 5.10: Monthly decadal trends at Torsvåg 1957-2005, given in %.

Month	CodUVAB	CodUVB	UV-A	UV-B	O_3
January	-	-	-	-	-
February	+3.6	+6.7	+1.4	+6.5	-2.1
March	+7.1	+9.3	+2.0	+14.2	-2.8
April	+ 6.9	+9.8	+1.7	+10	-2.3
May	+4.2	+5.3	+1.7	+ 5.2	-1.5
June	+ 3.1	+ 3.5	+ 1.9	+3.3	-0.8
July	+1.8	+2.5	-0.1	+2.3	-1.5
August	+ 1.8	+2.0	+1	+1.9	-0.6
September§	+ 3.1	+ 3.8	+1.8	+3.6	-0.7
October∗	+1.6	+1.0	+1.7	+1.2	+0.4
November∗	+0.5	-0.1	+1.1	-0.1	+0.1
December	-	-	-	-	-

∗trends only for 1957-2002.
§trends only for 1957-2003.

5.3 The Cod Index

This section first presents the main parameters governing the Cod Index (cloud cover, total ozone, cod weighted radiation at sea surface and wind) and the resulting cod indices for each station, The decadal trends of the yearly Cod Index for the spawning period are discussed. Finally the calculated overall Cod Index for the Arcto-Norwegian cod egg population is presented and compared to year class data.

5.3.1 Stationwise Cod Index

Cod weighted radiation at the sea surface, total cloud cover, total ozone content and mean wind speed for the different stations are shown separately to investigate the spatial variability and the influence of the different components on the Cod Index. All variables are shown as yearly values which are the sums of the daily means, Gaussian weighted according to the spawning period (see Chapter 3.4.4).

The total ozone content is shown in Figure 5.5 for northern and southern stations. Even though the Cod Index is calculated with different ozone data sets for the two southern stations, only one data set is shown here, as the data are quite similar. Total cloud cover in Figure 5.6 does not give a complete description of the cloud conditions, but it is at least a good indication of the cloud effect expected to be seen in the cod weighted radiation. As total cloud cover and total ozone are the main parameters determining cod weighted radiation at sea surface shown in Figure 5.8, the variations in these components are discussed in relation to variations in radiation levels. The wind conditions that influence the vertical distribution of cod eggs by turbulent mixing (Chapter 3.4.3), are shown in Figure 5.7. Together with the radiation this is the main parameter determining the Cod Index.

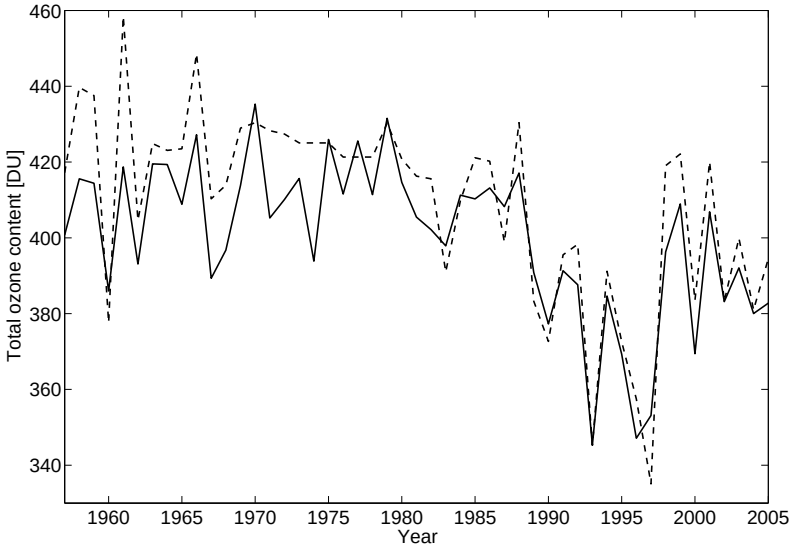

Figure 5.5: Total ozone content, Gaussian weighted according to the spawning period for 1) northern stations (line), 2) and southern stations (broken line)

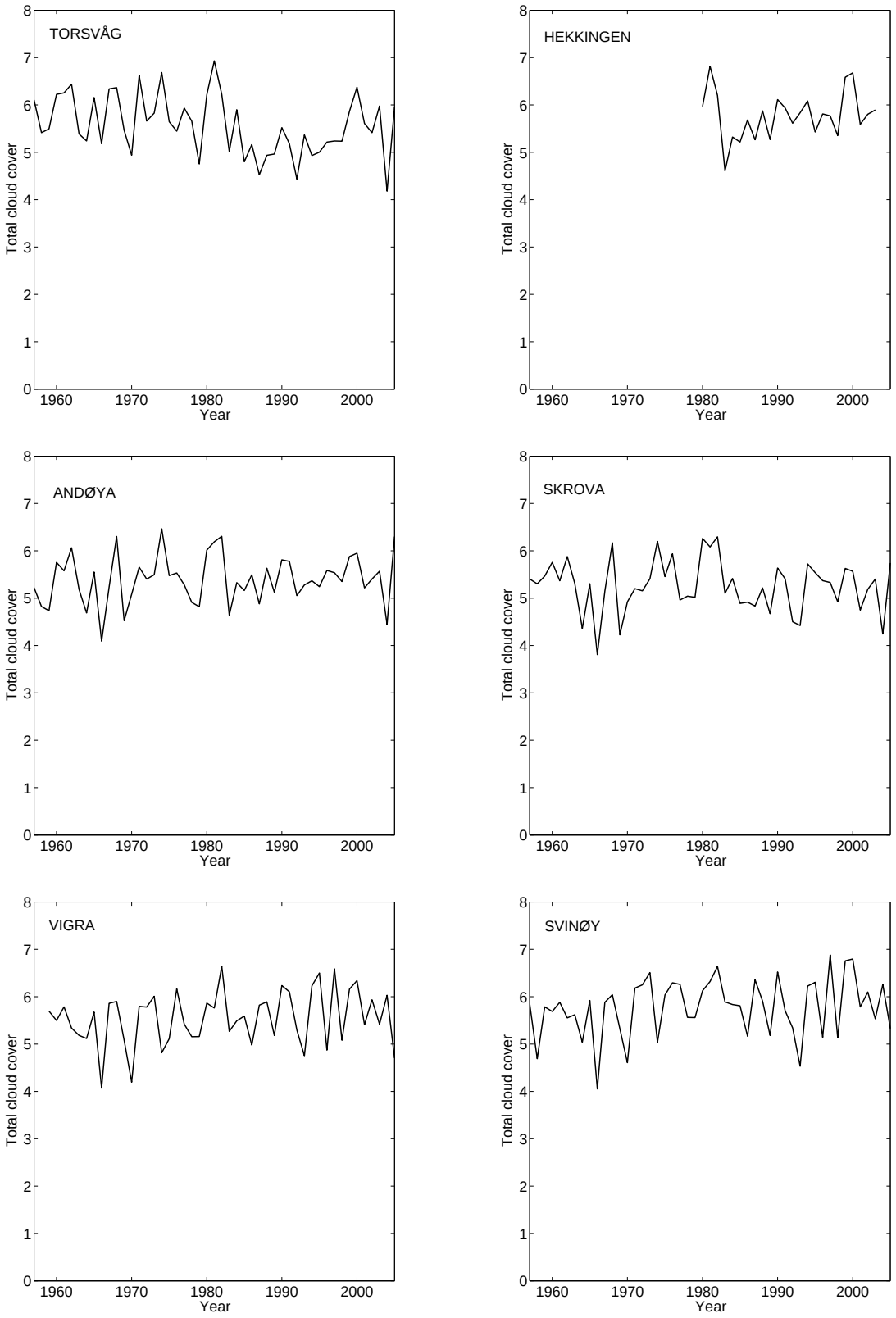

Figure 5.6: Total cloud cover, Gaussian weighted according to the spawning period for the different stations.

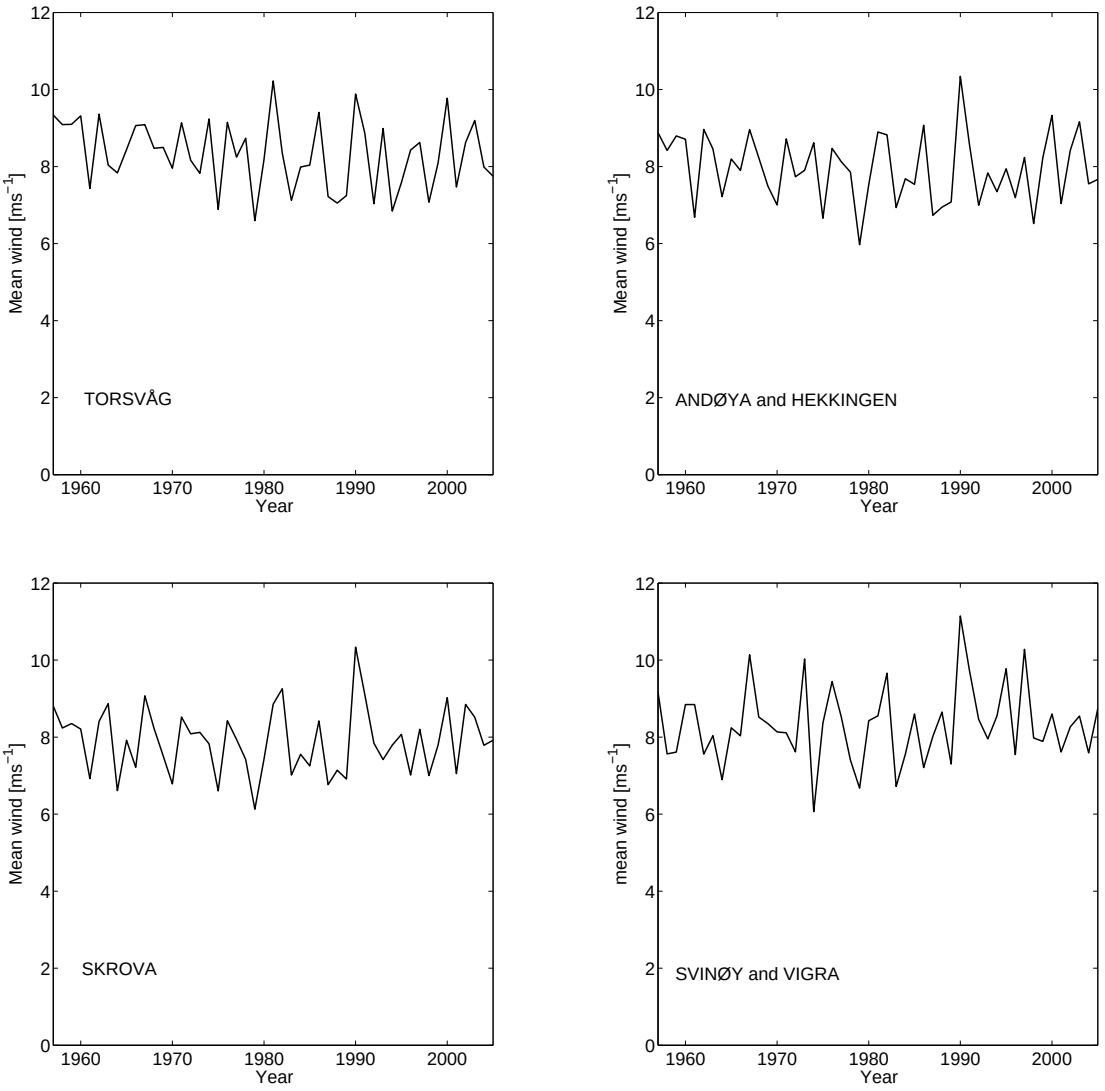

Figure 5.7: Mean wind speed, Gaussian weighted according to the spawning period for the four different locations chosen to describe the wind field: Vigra and Svinøy (62^o N, 4^o E), Skrova (68^o N, 14^o E), Andøya and Hekkingen (69^o N, 15^o E), and Torsvåg (70^o N, 19^o E).

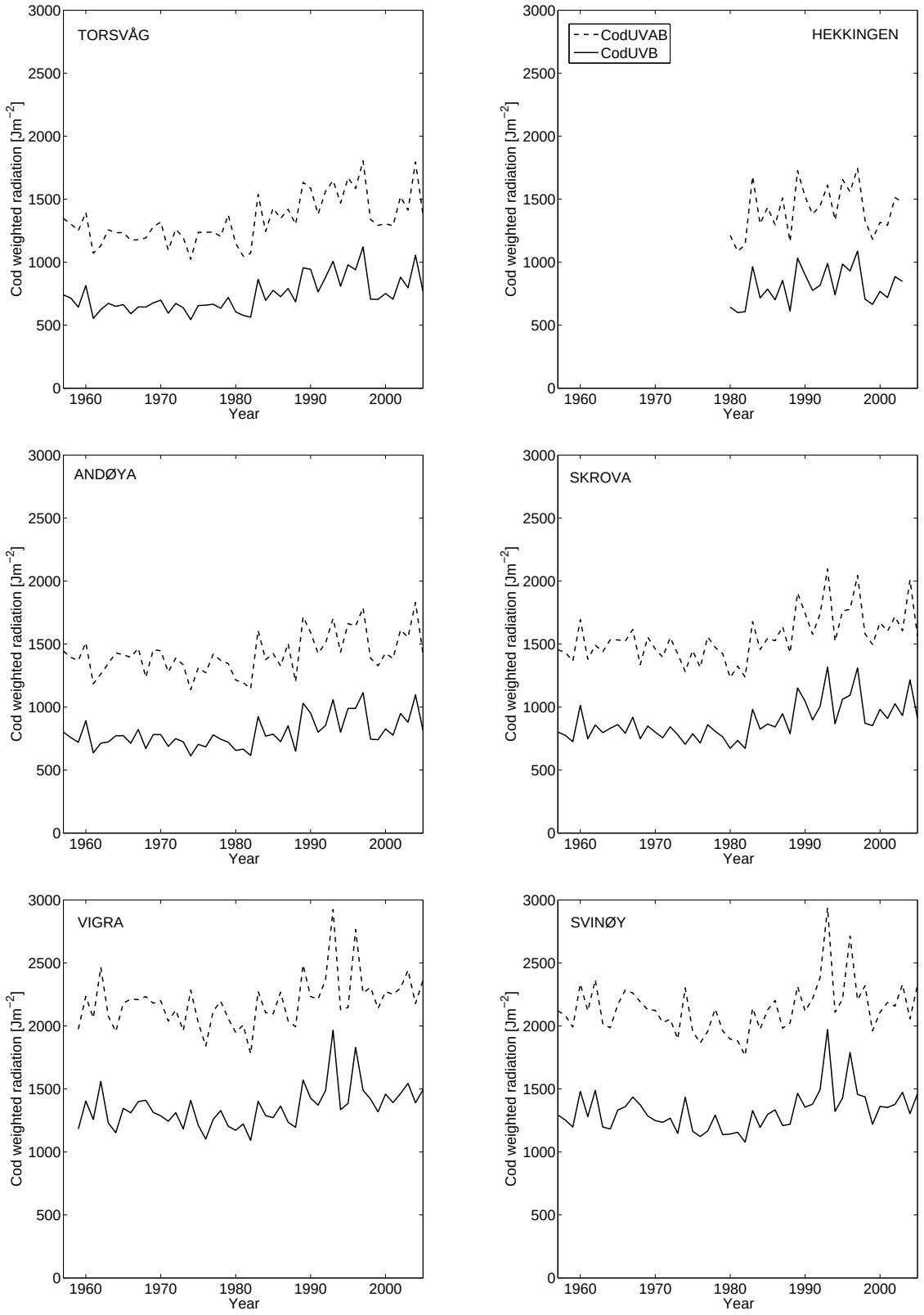

Figure 5.8: Cod weighted radiation at the sea surface, Gaussian weighted according to the spawning period for the different stations.

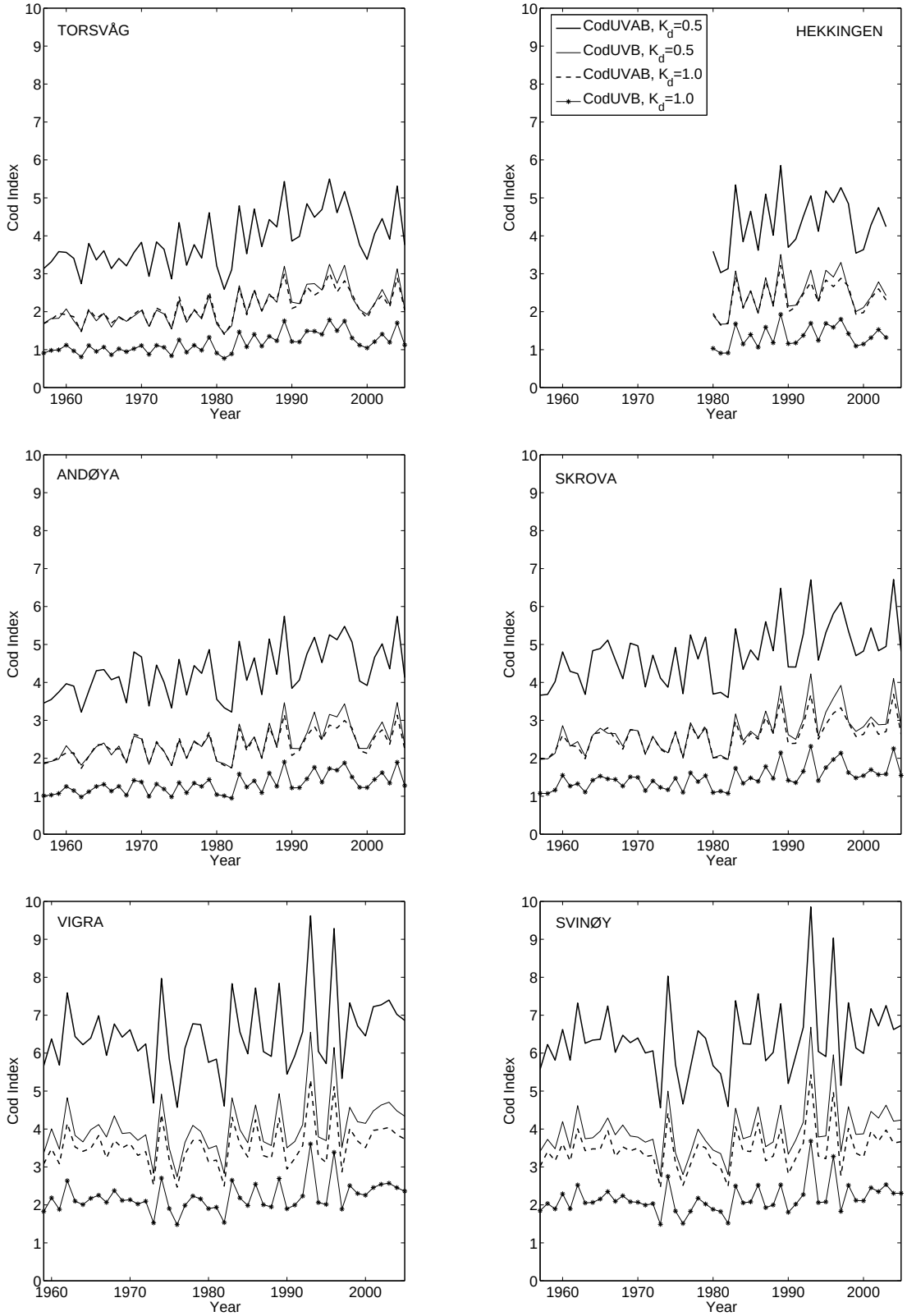

Figure 5.9: The Cod Index for the different stations shown for CodUVAB and CodUVB with high (K_d=1.0) and low (K_d=0.5) extinction coefficients of UV radiation in sea water.

Finally, the overall Cod Index for each station is shown in Figure 5.9. The index is shown for both UV-A and UV-B together and for UV-B alone for two different extinction coefficients for UV radiation in sea water ($K_d = 0.5$, $K_d = 1.0$, see Chapter 3.4.2). The Cod Index is scaled (divided by 10000) for following use in figures and tables.

The cod indices at all stations show relatively large yearly variations, where most maxima seem to occur after 1980 and minima before 1980. Looking at the variables (ozone, clouds, radiation and wind) most years with very low or high values of the Cod Index correspond to extremes in radiation. It is hard not to notice a common prominent minimum in 1982 for all stations with minima at the northern stations in 1980-1981 as well. This coincides with low radiation levels, which seem to be a combination of relatively high values of ozone and a large cloud fraction. But, Figure 5.7 shows large yearly variations in the wind conditions for the spawning period, and according to Chapter 3.4.3 high wind speeds causes mixing of the eggs in the vertical, which causes a considerably weakening in the exposure of UV radiation. To investigate and illustrate the effect and weight of each variable of the Cod Index, all variables and the cod indices at Svinøy and Andøya are shown for 1990-1999 in Tables 5.11 and 5.12. The tables show the percentage deviation of each parameter from the mean for this period. One station for the southern and one for the northern area are selected because the largest differences are seen between north and south. The period 1990-1999 is chosen because relatively large variations are observed here.

Southern stations, 62.33-62.56 ^{o}N

Table 5.11: Different parameters from Figures 5.5-5.9 for Svinøy given as percentage deviation of the mean of the parameters for the chosen priod 1990-1999. O_3 : Ozone, Cl: total cloud cover, W: wind, R: radiation, CI: Cod Index.

	90	91	92	93	94	95	96	97	98	99
O_3	+0.3	+4.1	+3.1	- 8.2	+2.3	-1.8	-7.7	-6.1	+5.4	+8.7
Cl	+11.4	-2.6	-8.8	-22.6	+6.4	+7.7	-12.2	+17.6	-12.4	+15.4
W	+24.8	+8.9	-5.2	-10.9	-4.3	+9.5	-15.5	+15.1	-10.7	-11.7
R	-8.8	-7.1	+0.5	+32.8	-11.0	-3.9	+20.5	-1.9	-3.2	-17.9
CI	-23.0	-14.4	-3.5	+54.3	-12.5	-11.9	+37.5	-21.4	+5.9	-10.9

As seen in Table 5.11 years with high deviations in the radiation values are recognized as years with high deviations in cloud cover and/or total ozone. When these two effects coincide the deviation is amplified. In 1993 for example, low ozone values coincide with low values of total cloud cover and therefore a large positive deviation in radiative values as seen here. Years with a low Cod Index mostly merge with years with low radiation and visa versa, but this only happens when wind conditions are average or near average. In 1998 there is a high negative wind deviation. This indicates little

turbulent mixing, giving a positive deviation in the Cod Index despite of the deviation in radiation being slightly negative. The wind effect is also prominent when looking at 1993 again when a high negative deviation in wind coincide with the high radiation values commented above. This results in an amplified positive deviation in Cod Index. The opposite effect is recognizable for 1990 when high wind values coincide with negative values of radiation resulting in an amplification of a negative deviation in the Cod Index.

Northern stations 68.15-70.25 ^{o}N

Table 5.12: Different parameters from Figures 5.5-5.9 for Andøya evaluated as percentage deviation of the mean of the parameters for the chosen priod 1990-1999. O_3 : Ozone, Cl: total cloud cover, W: wind, R: radiation,CI: Cod Index.

	90	91	92	93	94	95	96	97	98	99
O_3	-2.2	+3.8	+4.6	-9.4	+2.7	-2.2	-6.2	-12.0	+10.0	+10.8
Cl	+5.9	+5.3	-7.9	-3.8	-2.2	-4.5	+1.8	+0.9	-2.5	+7.1
W	+30.6	+8.2	-11.7	-1.1	-7.3	+0.3	-9.2	+4.0	-17.7	+3.9
R	+5.3	-11.5	-5.5	+17	-11.4	+9.4	+9.4	+23.2	-17.7	-18.1
CI	-18.0	-18.3	-3.4	+16.6	-9.1	+14.5	+12.1	+24.5	-1.1	-18.0

The Cod Indices at the northern stations are dampened compared to the southern stations due to lower radiation levels (see Figures 5.8 and 5.9). But as observed for Svinøy above, years with high deviations in the radiative values for Andøya in Table 5.12 are found for years with high deviations in cloud cover and/or total ozone. E.g. very low ozone values occur in 93 and 97 with corresponding higher values of radiation and Cod Index. As there were no prominent deviations in the wind for these two years the connection between radiative values and the Cod Indices is strong. In 1990 there is a very high positive deviation in wind, so despite a positive deviation in radiation, the deviation in the Cod Index is negative. This is an excellent example of the effects wind has on the vertical distribution of the cod eggs and hence the exposure to UV as described in Chapter 3.3.

5.3.2 Trends in Cod Index

Table 5.13 shows trends for cod weighted radiation in the UV-B area and the combination of UV-A and UV-B radiation for two different extinction coefficients of sea water (K_d = 0.5 and K_d= 1.0). In the following Cod weighted UV-B radiation will be emphasized.

Table 5.13: Decadal trends of the yearly Cod Index for the spawning period (10th of March-10th of May), given in %. Cod Index shown for CodUVAB and CodUVB with high (K_d=1.0) and low (K_d=0.5) extinction coefficients of UV radiation in sea water.

Station	**Period**	**CodUVB k=0.5**	**CodUVB k=1**	**CodUVAB k=0.5**	**CodUVAB k=1**
Svinøy	1957-2005	+4.1	+4.2	+2.6	+2.6
	1957-1982	-5.5	-5.5	-5.0	-5.0
	1983-2005	+3.6	+3.6	+1.4	+1.4
	1982-2005	+7.1	+7.1	+4.7	+4.7
	1980-2005	+9.3	+9.4	+6.7	+6.8
Vigra	1959-2005	+4.9	+4.9	+3.3	+3.3
	1959-1982	-5.6	-5.8	-4.8	-4.9
	1983-2005	+4.7	+4.7	+2.4	+2.4
	1982-2005	+8.3	+8.3	+5.8	+5.8
	1980-2005	+10.1	+10.1	+7.4	+7.4
Skrova	1957-2005	+10.2	+10.3	+7.1	+7.3
	1957-1982	-0	+0.3	+0.5	+0.8
	1983-2005	+5.7	+5.7	+3.6	+3.6
	1982-2005	+9.3	+9.4	+6.8	+6.8
	1980-2005	+14.5	+14.6	+11.1	+11.2
Andøya	1957-2005	+9.4	+9.7	+6.7	+6.9
	1957-1982	+1.5	+1.9	+1.8	+2.2
	1983-2005	+4.0	+4.0	+2.3	+2.2
	1982-2005	+7.6	+7.6	+5.5	+5.5
	1980-2005	+12.1	+12.2	+9.4	+9.5
Hekkingen	1980-2005	+9.8	+9.9	+6.7	+6.9
Torsvåg	1957-2005	+12.3	+12.5	+9.3	+9.5
	1957-1982	+0.5	+0.8	+1.2	+1.5
	1983-2005	+0.3	+0.2	-1.0	-1.1
	1982-2005	+4.0	+3.8	+2.2	+2.0
	1980-2005	+10.5	+10.5	+8.0	+7.9

As shown in Tables 5.11 and 5.12, both radiation at the sea surface and wind conditions are the dominating effects. Analysis of the yearly wind values in Figure 5.7 showed that the trends are negligible. Therefore, as relatively strong positive trends were observed for radiative data in Tables 5.5-5.10, the trends of the Cod Indices are expected to be similar to these.

The discussion of trends in UV radiation and ozone in Chapter 5.2 showed that there is an alteration in the trends for spring months when comparing the northern stations with data from 1957-2005 (Tables 5.7, 5.8 and 5.10) with Hekkingen (Table 5.9) with data for only 1980-2003. The decadal trends for the Cod Indices in Table 5.13 are therefore calculated for different periods. As relatively low Cod Index values were observed at all stations in the early 1980s (see Figure 5.9), trends for the second half period was calculated with different starting years. This illustrates the sensitivity of the calculation in trends on the selected time period.

For the southern stations there is a positive decadal trend in cod weighted UV-B radiation for the period 1957-2005 of +4.1 to +4.9 %. The first half of the period (1957-1982) shows a negative decadal trend of -5.5 to -5.8 % while the second period is always positive independent on the choice of starting point with positive trends of +3.6 to +10.1 %. The years 1980-1982 seem however to be minimum points as the trend increases considerably when including these years.

For the three northern stations with data 1957-2005 the trends for cod weighted UV-B radiation are in the range +9.4 to +12.5 %. When dividing the period in two the trends for the first period are relatively insignificant (0 to +1.9 %), while the second period is, as for the southern stations, always positive with the strongest trends when including 1980 (+10.5 to +14.6 %). Also as for the southern stations, the trends change dramatically when including different years, this is due to the very low values in the Cod Index mentioned in Chapter 5.3.1. The abrupt change in trends could indicate a flattening in the yearly Cod Index. Nevertheless the recent UV exposure of cod eggs is higher than before 1980.

As the majority of spawning has occurred in northern territories (Table 3.1), the trends for the northern stations are of particular interest. The positive trends in the cod indices at these stations indicates that the trend in the overall is positive as well.

5.3.3 Overall Cod Index

The yearly overall Cod Index for the Arcto-Norwegian cod egg population is calculated as described in Chapter 3 and shown below in Figure 5.10. Also, the trends in the overall Cod Index for the different periods given in Table 5.13 are shown in Table 5.14.

As the major known biological effect of radiation on cod occur in the UV-B area (see Chapter 3.3) further discussion only include plots of cod weighted radiation within the UV-B region. The largest extinction coefficient (K_d=1.0) is also excluded, which leaves the data on CodUVB, (K_d=0.5), left for discussion.

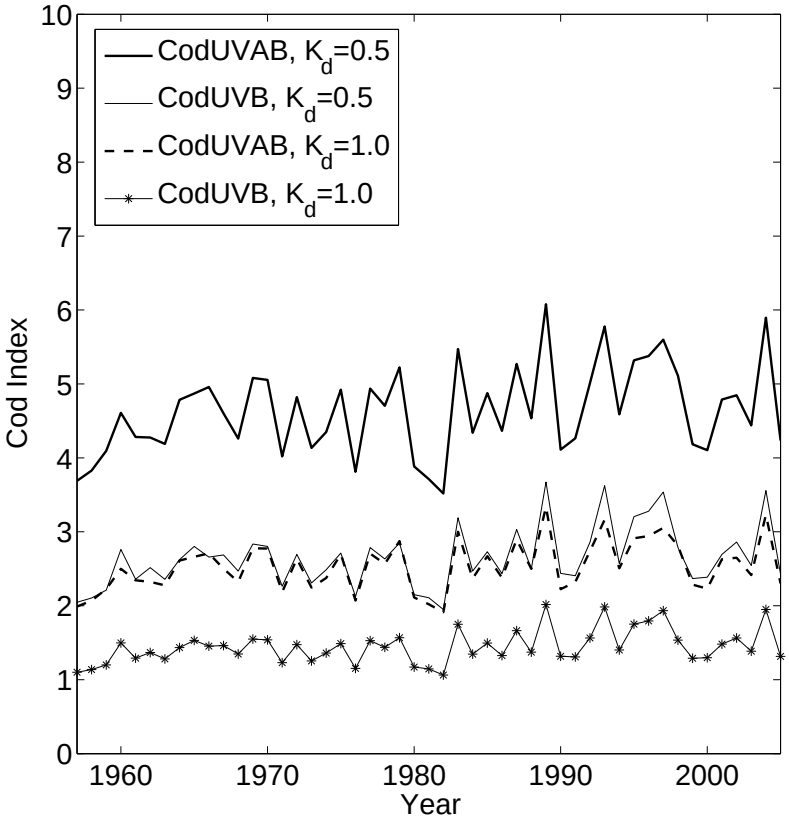

Figure 5.10: Overall Cod Index for the Arcto-Norwegian cod egg population weighted according to spawning sites according to Table 3.1. Shown for CodUVAB and CodUVB with high (K_d=1.0) and low (K_d=0.5) extinction coefficients.

Table 5.14: Decadal trends of the yearly Cod Index for 1957-2005, given in %.

	1957-2005	**1957-1982**	**1980-2005**	**1982-2005**	**1983-2005**
CodUVB K_d=0.5	+4.8	-0.2	+7.2	+3.3	-0

As expected, the overall Cod Index appears similar to the Cod Indices for the northern stations, Andøya and Skrova in particular, as they are strongest weighted in the final Cod Index (see Table 3.1 for details). The trends shown in Table 5.14 are also similar to the trends shown for each station in Table 5.13, but weaker. The five highest

maxima in the overall Cod Index occur after 1980, but the yearly variations are great, as observed at each station (Chapter 5.3.1). Even if the trends vary when including different years, there is an existing positive trend in the Cod Index for the total period 1957-2005 (+4.8 %), hence there has been an increasing exposure of UV radiation on cod eggs during the past 49 years.

It should, however, be mentioned that according to Table 3.1 there are indications of the cod preferring spawning-areas in more northerly areas, when temperature increases. Because of an expected temperature increase in the ocean, the cod is expected to spawn even further north than present day in the future (Stenevik and Sundby, 2007). If the cod goes further north it automatically moves to spawning areas with lower radiation. This will lead to a moderation in the Cod Index from Figure 5.10, hence smaller potential UV effects. In addition, as mentioned in Chapter 5.2, the total column ozone for the Northern Hemisphere has increased slightly during the last decade, leading to a corresponding decrease in UV radiation for the future (Chipperfield and Fioletov, 2007; Bais and Lubin, 2007).

5.3.4 Effect on Year Class

One important aim of this study is to investigate if UV radiation has any effect on the amount of year class cod. The year class strength of cod is mainly determined after the three month period of the egg, larvae and early juvenile stage, but the mortality is at its highest during the eggs stage (Chapter 3.2). If UV exposure induces mortality, the variability in the Cod Index could be recognizable in the strength of year class cod. As presented in Ellertsen et al. (1989), there is a connection between mean sea temperature at 0-50 meters depth for March and April at Lofoten and the strength of year class of Arcto-Norwegian cod. The study shows no functional relationship, but the plot of the year class versus the temperature indicates that years with high sea temperatures give year class strengths in the whole range, but at low sea temperatures, the year classes are always small. These results are shown in Figure 5.11, where also data until 2002 are added. Because the sea temperature seem to be a dominating factor, UV induced mortality can be difficult to identify.

At the moment, data on year class size only exist for up to 2002. Thus, even if this study has produced cod indices for up to 2005, the following discussion only includes the period 1957-2002.

To possibly identify and perhaps separate the UV effect from the observed temperature effect, time series and scatter plots are shown for comparisons of the overall Cod Index, year class size and sea temperature in Figure 5.12. The scatter plot of temperature vs year class shown in Figure 5.12 is identical to Figure 5.11, but restricted to the period of interest in this study, 1957-2002. When studying these plots it is important to keep in mind that in addition to the temperature dependency described above, it is to be expected that the high fishing pressure with decline in spawning stock biomass in the recent years, particularly from 1990s, also has influenced the abundances of recruiting

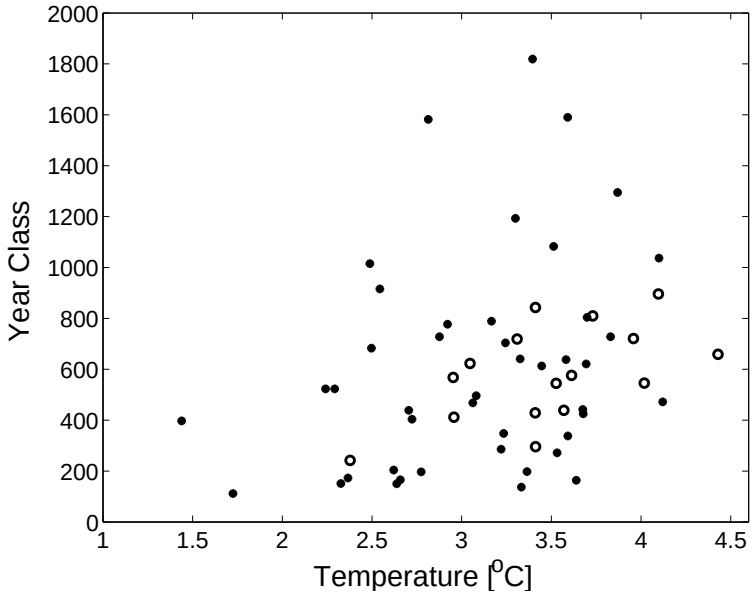

Figure 5.11: Year class data of cod vs mean sea temperature for March/April at 0-50 meters depth in Lofoten. Filled symbols are year class and temperature for 1943-1986, compatible with data presented in Ellertsen et al. (1989). Open symbols present data from 1987-2002

.

year classes (personal correspondence, Svein Sundby). In addition, the age at maturation has steadily declined since 1950s, from about 11 years to just above six years today. Small and young cod are producing far less eggs than the older and bigger ones, and there are indications of that the smaller ones tend to swim shorter distances and consequently prefer northern spawning territories (personal correspondence, Svein Sundby). To compare variables and examine the correlations with and without the influence of over-fishery, Figure 5.13 shows data from Figure 5.12 divided into two periods; one period before and one after over-fishery becomes an issue. In addition, correlation coefficients and averages for each value for these two periods and the whole period are shown in Table 5.15 and 5.16.

For the whole period 1957-2002, a correlation coefficient of 0.3, significant on a 0.05 level, is found between year class and sea temperature (Table 5.15). From Figure 5.12 it is also seen that strong year classes never appear at low temperature, and that the lowest year classes do not appear at the highest temperatures. When separating data from years where over-fishery has been an issue, the period 1957-1990 shows a correlation coefficient of 0.33, but for the period 1991-2002 there is a lower correlation coefficient of 0.1 between year class and temperature (neither were significant on a 0.05 level). According to Table 5.16 the period 1991-2002 has higher average sea temperature and year class than the period 1957-1990. The higher temperature corresponds well to the general trend in mean sea temperature described in Chapter 3.4.4. Nevertheless, even though the average sea temperature is higher for 1991-2002 than for 1957-1990, the year classes are only moderate to low for this period (Figure 5.13). High fishing

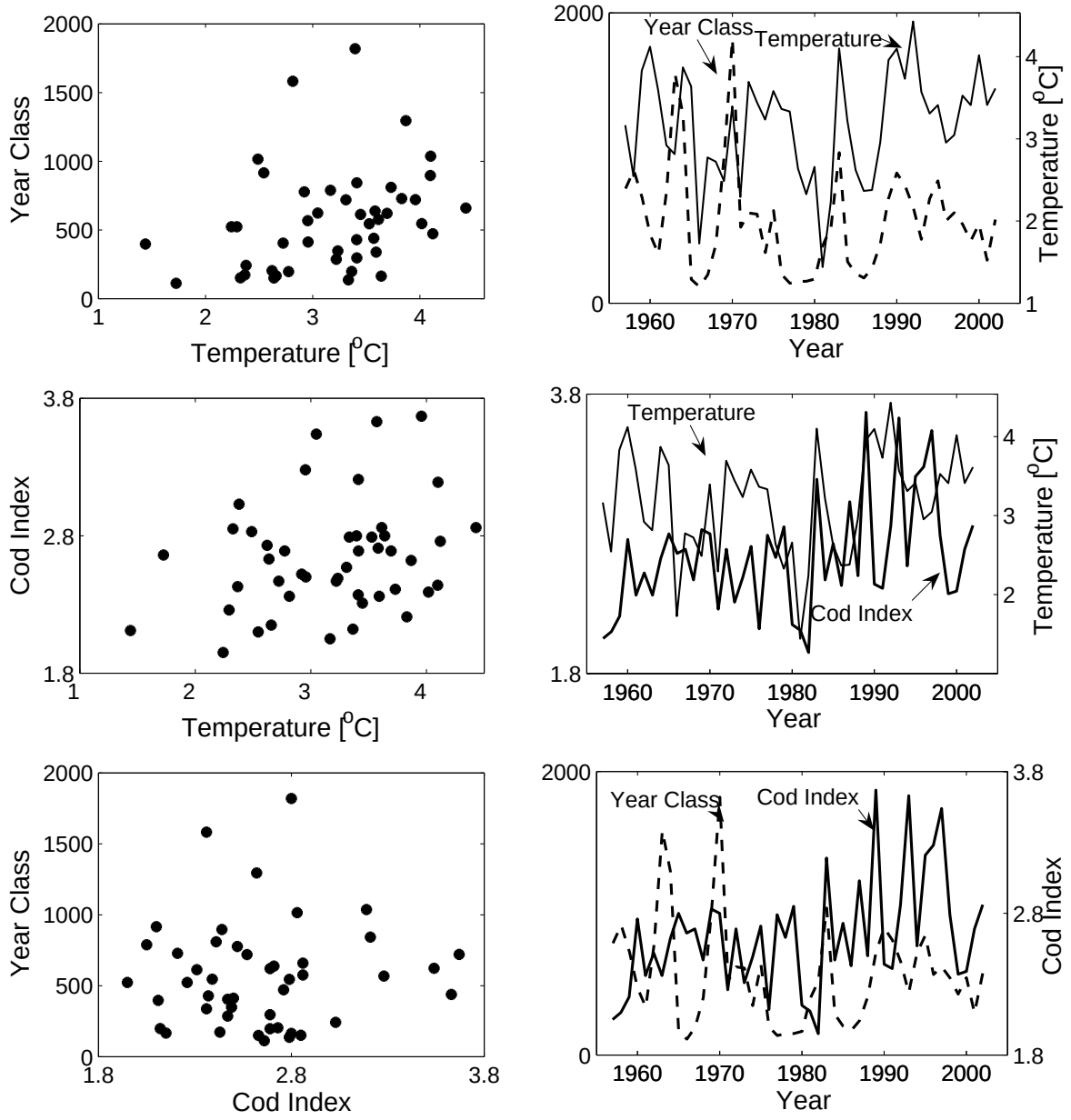

Figure 5.12: Scatter plot (left column) and time series (right) of year class and sea temperature (top), Cod Index and mean sea temperature (middle), year class and Cod Index (bottom).

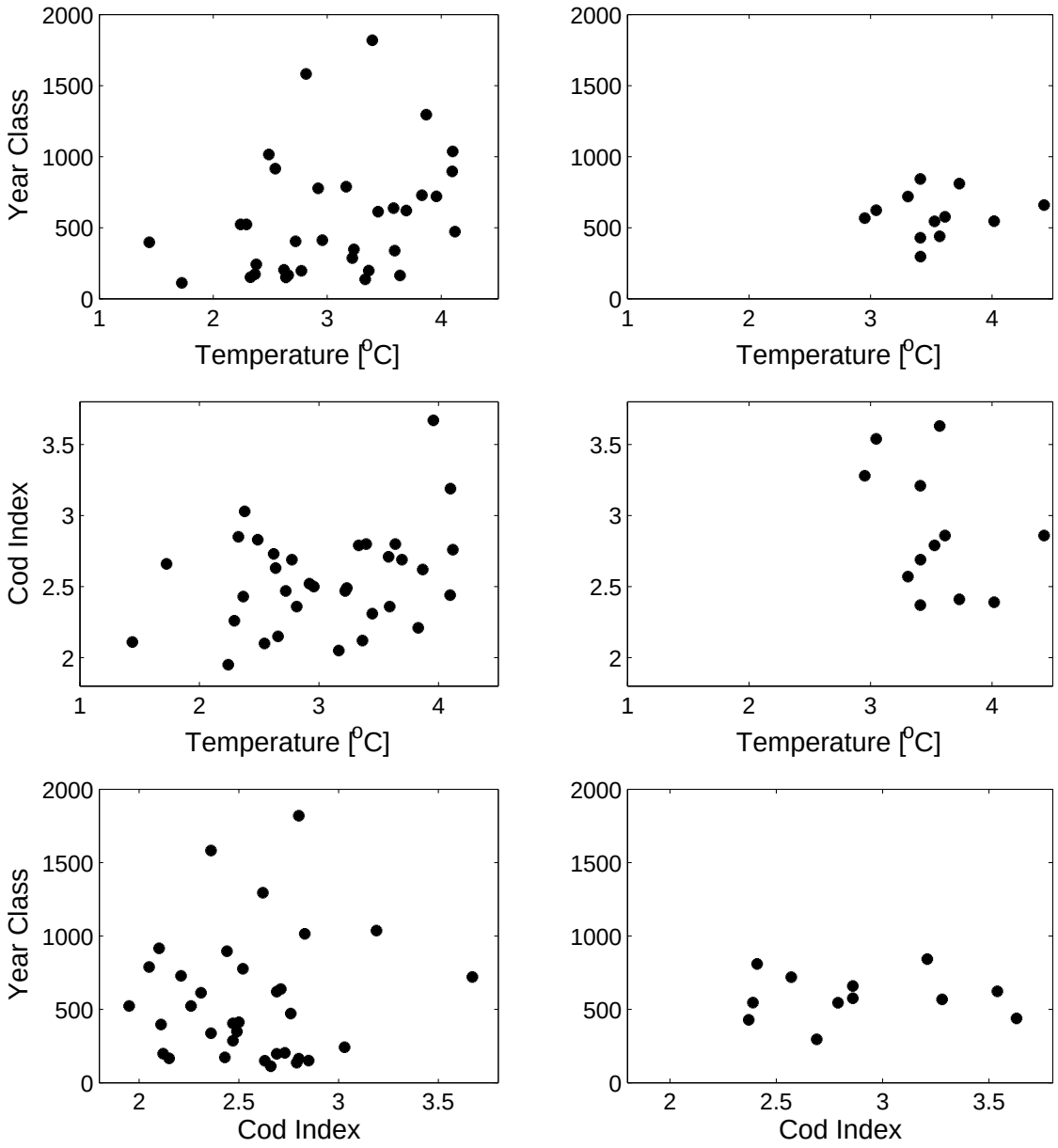

Figure 5.13: Plots corresponding to the scatter plots in Figure 5.12 but divided into two periods; 1957-1990 (left) and 1991-2002 (right).

Table 5.15: Correlation coefficients. The whole period: 1957-2002, before over-fishery: 1957-1990, with over-fishery included: 1991-2002. Correlation significant on a 0.05 level is shown in bold writing.

	1957-2002	**1957-1990**	**1991-2002**
Year Class vs Sea Temperature	**0.31**	0.33	0.10
Sea Temperature vs Cod Index	0.28	0.33	-0.39
Year Class vs Cod Index	0.06	0.06	+0.00

pressure, most likely limits the possibility of strong year classes in this period. Even though all year classes after 1990 lies within a narrow range of moderate to low values, the average year class strength shown in Table 5.16 is highest for this second period. Higher sea temperatures seem in a way to be favourable for the cod, but it is important to keep in mind that there are other limiting factors.

According to Figure 5.12 there seems to be a relationship between sea temperature and Cod Index, and there is a correlation coefficient of 0.3 for the whole period as shown in Table 5.15 (not significant on a 0.05 level). High cod indices mostly occur in years with high temperatures, while low cod indices occur at any temperature. There is however, no reason to believe that these two parameters are correlated. While sea temperature is determined by large scale processes (Gill, 1982), the Cod Index is determined by processes with a higher temporal and spatial variability (shown in Chapter 5.3). With a few exceptions, most high temperature and most high cod indices are seen for the years after 1991 (Figures 5.10 and 5.13). High cod indices are seen for this period in Figure 5.10, and the Cod Index average shown in Table 5.16 is higher after 1990 than before. The shift in correlation coefficient from positive to negative in Table 5.15 is therefore believed to be random.

Year class and Cod Index in Figure 5.12 do not seem to be correlated, and the correlation coefficient in Table 5.15 is thus close to zero. It is however, possible to recognize a certain pattern; large year classes only occur with intermediate values of the Cod Index and the lowest year classes do not occur for high cod indices. Here, one must keep in mind that the last period with higher Cod Index, is affected by over-fishery. This pattern could indicate that intermediate values of the Cod Index is favourable for the cod egg population, but the pattern could also be random as this study only includes data from 46 years (1957-2002), where roughly one third of the period is strongly regulated by high fishing pressure.

Even if no specific correlation or connection is observed between the year class strengths and the Cod Index for this study, the results do not reject the idea of UV radiation

Table 5.16: Averages of year class strength (in millions), mean sea temperature [^{o}C] (see Chapter 3.5) and Cod Index for the periods 1957-1990 (before over-fishery) and 1991-2002 (with over-fishery).

	1957-1990	**1991-2002**
Year Class	560	588
Sea Temperature	3.0	3.5
Cod Index	2.6	2.9

causing detrimental effects on the cod eggs. Tables 5.5-5.10 showed that there has been a significant increase in UV-B radiation for the main spawning areas, and no trend is observed for wind conditions for the spawning period (Figure 5.7, Chapter 5.2). Thus, when excluding yearly variations in the wind, the positive trend in UV-B radiation has led to increasing exposure of UV radiation on the cod egg population, as reflected in the overall Cod Index (Table 5.14).

Many studies have, however, concluded that cod eggs are insensitive to daily levels of UV radiation. Eilertsen et al. (2007) and Kuhn et al. (2000) both found that the UV induced mortality of cod eggs is insignificant unless extreme meteorological conditions with high UV radiation and slack winds occur, conditions seldomly seen for these geographical areas. These studies investigate cod egg mortality per day, while the Cod Index is a weighted mean illustrating the yearly exposure of UV radiation on the Arcto-Norwegian cod egg population. Therefore, a direct parallel and comparison can not be drawn between the result of these studies and the lack of correlation of year class and Cod Index.

The lack of a correlation between year class and Cod Index does, however, suggest that other factors are more dominant for the year class, as sea temperature (Ellertsen et al., 1989) or human interference as over-fishery. Also, UV radiation might have a greater effect on other components of the cod ecosystem. Browman et al. (2000) and Kuhn et al. (2000) showed that UV induced mortality in Calanus Finmarchicus, the primary prey of the cod larvas, is higher than for cod eggs. This idea is also indicated in a EU-project (UVAC project, 2003) that performed a correlative analysis of UV radiation and biological data of cod and Calanus Finmarchicus. The results showed no direct negative correlation with cod recruitment, but rather indicated a negative correlation between UV radiation and the Calanus Finmarchicus population strength. It was suggested that UV radiation reduces summer reproduction of Calanus Finmarchicus causing a population decline, hence reducing the food abundance in the spawning habitats in the following spring.

The method for calculating the Cod Index is a new method to map UV effects on the cod egg population and is, if proper data are available, easiliy applied to other aquatic organisms. In the future the Index may be applied to the Calanus Finmarchicus population and examine the possibilities of an effect on year class strength of cod.

Chapter 6

Summary and conclusion

The main purpose of this study was to reconstruct UV radiation and express the yearly UV exposure of the Arcto-Norwegian cod egg population for 1957-2005 as a Cod egg UV Index (Cod Index), developed by a new method.

The method for calculating the Cod Index includes the actual exposure of biological weighted radiation when considering the vertical mixing of the cod eggs and UV transmissivity in sea water (λ= 305 nm). The vertical mixing depends mainly on surface wind conditions. A formulae for cod egg concentration adapted from the work of Sundby (1983) is used to express the vertical cod egg profile as a function of wind speed. The biological weighting of the UV radiation is described using a biological weighting function derived by Kouwenberg et al. (1999a), while UV transmittance in sea water is approximated based on existing literature (Erga et al., 2005).

To apply the Cod Index to the Arcto-Norwegian cod egg population, information on the temporal distribution of the cod eggs within the spawning period (10th of March-10th of May) is needed. Also, the temporal and spatial spawning behavior for the last 49 years and reconstructed UV radiation for the current spawning areas was included. As the overall spawning area is divided into six areas, UV was reconstructed for six SYNOP stations. Much work was invested into collecting and processing the cloud observations needed to reconstruct UV radiation. For the reconstruction some assumptions were made (albedo=0.03, maritime clean aerosol type) to provide the necessary input data in the model STAR. The observed wind data were sparse, so wind data from the Hindcast database for locations off shore were used instead. The wind values were validated through a comparison to observed values. The Hindcast data had an even overestimation, but this can be expected, as the observation stations are located on shore with surrounding topography and thus possible sheltering effects.

To investigate the quality of the reconstructed UV radiation, such data at Andøya were compared to observed values for the period 2000-2004. The comparison between modelled and observed daily erythemal UV doses for the individual years all showed correlation coefficients of 0.94-0.97, for the total period the correlation coefficient was 0.96, which is considered acceptable. For hourly values somewhat lower correlation coefficients, 0.90-0.93, and a certain spread was present. This was, however, expected

mainly as no information of global radiation was included in the modelling. For the spring season daily and hourly values showed correlation coefficients of 0.95 and 0.92, respectively. Besides, in spring, the regression line between reconstructed and observed daily values coincide with the 1 -to- 1 line, which is most satisfactory and the UV radiation reconstructed for the spawning season can therefore be considered as excellent.

The trends in UV-B radiation were positive for all spring months at the five stations with data for the whole period 1957-2005, and the strongest trends were observed for the three most northern stations with trends between +7.2% and +14.2% for March and April. The trend for Hekkingen, with data only for 1980-2003, was positive in April, but slightly negative for March and May. May had only weak trends at all stations, but as the spawning season is defined as 10th of March-10th of May, the conclusion is that there are positive trends for UV-B in spawning season at all stations. The strong trends in UV-B radiation are strongly regulated by a corresponding decrease in ozone, where the decrease is strongest for the northern stations. Some months at various locations have a positive trend in UV-A radiation, indicating a decrease in cloud extinction.

The Cod Index was calculated for both UV-B (codUVB) and for the sum of UV-A and UV-B (codUVAB), and for two extinction coefficients of UV radiation in sea water. As the major effects are found within the UV-B area CodUVB was used for the determination of the overall Cod Index. Firstly, the yearly Cod Index was shown for each of the six SYNOP stations. The relevant variables such as ozone, total cloud cover, wind and radiation were presented separately to evaluate which parameter determines the year to year variability in the Cod Index. Years with a high Cod Index often coincided with high radiation, but when strong wind conditions were present, the Cod Index was considerably weakened.

All stations showed positive decadal trends in the cod index (+4.1 to +12.5 %) for the total period 1957-2005, where the northern stations had the strongest trends (+9.4 to +12.5 %). When dividing the period in two the decadal trends were somewhat higher for the second period. However, the trends were heavily dependent on even small adjustments of the time period. Trends in the wind conditions were negligible, hence the positive trends observed for UV radiation and thus for cod weighted radiation are the main cause for the increase in cod egg exposure to UV radiation.

The overall Cod Index was calculated by weighting the yearly Cod Index at each station according to the spatial and temporal distribution of the spawning. The decadal trend in the overall Cod Index varied for different subperiods, but was positive (+ 4.8 %) for the total period, 1957-2005. Hence there has been an increasing exposure of UV radiation on cod eggs during the past 49 years.

At last, the overall Cod Index was compared with year class data to investigate a possible correlation between them. A study of Ellertsen et al. (1989) showed a connection between year class and sea temperature. In this thesis a correlation coefficient of 0.3 significant on a 0.05 level was found. Year class vs the Cod Index was studied both for the whole period 1957-2002, but also for the two periods, 1957-1990 and 1991-2002

separately, as the last period is strongly affected by high fishing pressure in the Barents Sea. It was, however not possible to identify any correlation. A certain pattern was, however, present: strong year classes only occur for intermediate values of the Cod Index. Intermediate values of the Cod Index might thus be favorable for the cod egg population. This could also be random as this study only includes data from 46 years (1957-2002), where roughly one third of the period is strongly regulated by high fishing pressure.

Even if no specific correlation or connection is observed between the year class strengths and the Cod Index for this study, the results do not reject the idea of UV radiation causing detrimental effects on the cod eggs. The lack of a correlation does however, suggest that other factors are more dominant for the year class, as sea temperature (Ellertsen et al., 1989) or human interference as over-fishery. Recent studies have, however, concluded that cod eggs are insensitive to daily levels of UV radiation. Eilertsen et al. (2007) and Kuhn et al. (2000) both found that the UV induced mortality of cod eggs is insignificant unless extreme meteorological conditions with high UV radiation and slack winds occur, conditions seldomly seen for these geographical areas. A study by (Skreslet et al., 2005) have suggested that UV radiation might cause a positive effect in the way that UV-B reduce the amount of bacteria harmful for the eggs. But studies have also suggested that UV radiation effects other components of the cod ecosystem, such as Calanus Finmarchicus, the main prey of the cod larvas (Browman et al., 2000; UVAC project, 2003; Kuhn et al., 2000).

This work has produced Cod Indices and reconstructed UV radiation for the spawning areas for nearly five decades. For the future, these data may be used in studies of UV related topics or further investigations of the potential effects on the Arcto-Norwegian cod egg population. The algorithm for calculating the Cod Index developed in this work is a new method to investigate UV effects on aquatic biological systems. If proper data are available (e.g. BWF, buoyancy etc.), the method can easily be applied to other aquatic organisms. It is however important to keep in mind that biological systems are highly complex, and the effects of one specific parameter is hard to identify.

Bibliography

Bais, A. F. and Lubin, D. (2007), 'Surface Ultraviolet Radiation: Past, Present, and Future', *Meteorological Organization Global Ozone Research and Monitoring Project, No. 50* .

Bèland, F., Browman, H. I., Roderiguez, C. A. and St-Pierre, J.-F. (1999), 'Effect of solar ultraviolet radiation (280-400 nm) on the eggs and larvae of Atlantic cod (Gadus morhua)', *Can. J. Fish. Aquat. Sci. 56: 1058-1067* .

Browman, H. I., Roderiguez, C. A., Bèland, F., Cullen, J. J., Davis, R. F., Kouwenberg, J. H. M., Kuhn, P. S., McArthur, B., Runge, J. A., St-Pierre, J.-F. and Vetter, R. D. (2000), 'Impact of ultraviolet radiation on marine crustacean zooplankton and ichthyoplankton: a synthesis of results from the estuary and Gulf of St. Lawrence, Canada', *Marine Ecology Progress Series, Vol. 199: 293-311* .

Browman, H. I. and Vetter, R. D. (2002), 'Impacts of UV radiation on crustacean zooplankton and ichthyoplankton: case studies from subarctic marine ecosystems.', *UV Radiation and Arctic Ecosystems, pp. 261-297* .

Capone, A., Digaetano, T., Grimaldi, A., Habel, R., Presti, D. L., Migneco, E., Masullo, R., Moro, F., Petruccetti, M., Petta, C., Piattelli, P., Randazzo, N., Riccobene, G., Salusti, E., Sapienza, P., Sedita, M., Trasatti, L. and Ursella, L. (2002), 'Measurements of light transmission in deep sea with the AC9 trasmissometer', *Nuclear Instruments and Methods in Physics Research A 487, 423-434* .

Carlson, T. (2005), UV-stråling i Norge: Satellittestimater, modellestimater og bakkemålinger, Master's thesis, University of Bergen.

Cascinelli, N. and Marchesini, R. (1989), 'Increasing incidence of cutaneous melanoma, ultraviolet radiation and the clinician', *Photochem Photobiol. 50:497-505* .

Chipperfield, M. P. and Fioletov, V. E. (2007), 'Global Ozone: Past and Present', *WMO: Global Ozone Research and Monitoring Project, No. 50* .

Crutzen, P. J. (1974), 'Estimates of possible future ozone reductions from continued use of fluorochloromethanes (CF_2Cl_2 , $CFCl_3$)', *Geophys. Res. Lett., 1, 205-208* .

Eilertsen, H. C., Wyatt, T. and Hansen, E. (2007), 'Can ultraviolet radiation influence cod Gadus morhua L. year class strength: a model study', *Journal of Fish Biology, Vol. 70, p. 1120-1133* .

Ellertsen, B., Fossum, P., Solemdal, P. and Sundby, S. (1989), 'Relation between temperature and survival of eggs and first-feeding larvae of northeast Arctic cod (Gadus morhua L.)', *Rapp. P.-v. Reun. Cons. int. Explor. Mer, 191:209-219* .

Ellertsen, B., Furnes, G. K., Solemdal, P. and Sundby, S. (1981), 'Effects of upwelling on the distribution of cod eggs and zooplankton in Vestfjorden', *Proc. from Norwegian Coastal Current Symposium, Geilo, Norway, 9-12 September 1980 (Eds: R. Sætre and M. Mork.) University of Bergen: 604-628* .

Engelsen, O., Hansen, G. H. and Svenøe, T. (2004), 'Long-term (1936-2003) ultraviolet and photosynthetically active radiation doses at a north Norwegian location in spring on the basis of total ozone and cloud cover', *Geophysical reasearch letters, vol. 31, L12103, doi:10.1029/2003GL019241* .

Erga, S. R., Aursland, K., Frette, ., Hamre, B., Lotsberg, J. K., Stamnes, J. J., Aure, J., Rey, F. and Stamnes, K. (2005), 'UV transmission in Norwegian marine waters: controlling factors and possible effects on primary production and vertical distribution of phytoplankton', *Marine Ecology progress series, vol. 305: 79-100* .

Farman, J. C., Gardiner, B. G. and Shanklin, J. D. (1985), 'Large Losses of Total Ozone in Antarctica Reveal Seasonal ClO_x/NO_x Interaction', *Nature, May 16, pp 207-210* .

Fioletov, V. E., Kerr, J. B., Hare, E. W., Labow, G. J. and McPeters, R. D. (1999), 'An assesment of the world ground-based total ozone network perfomance from the comparison with satellite data', *Journal of geophysical reasearch, Vol. 104, Issue D1, p. 1737-1748* .

Gill, A. E. (1982), *Atmosphere-Ocean Dynamics*, Vol. 30 of *International geophysics series*, Academic Press.

Hartmann, D. L. (1994), *Global Physical Climatology*, Academic Press.

Häder, D.-P., Kumar, H. D., Smith, R. C. and Worrest, R. C. (1998), 'Effects on aquatic ecosystems', *Journal of Photochemistry and Photobiology B: Biology 46, 53-68* .

Häder, D.-P., Kumar, H. D., Smith, R. C. and Worrest, R. C. (2007), 'Effects of Solar radiation on aquatic ecosystems and interactions with climate change', *Photochem. Photobiol. Sci., 6, 267-285* .

http://alomar.rocketrange.no/guv.html (2007), 'ALOMAR Artic Lidar Observatory'.

http://ingrid.ldeo.columbia.edu/dochelp/StatTutorial/Interpolation/ (2007), 'The International Research Institute for Climate and Society'.

http://woudc.ec.gc.ca (2007), 'World Ozone and Ultraviolet Radiation Data Center'.

imr.no (2007), 'Institute for Marine Research, Bergen, Norway', *www.imr.no* .

Iqbal, M. (1983), *An introduction to Solar Radiation*, Academic Press.

Josefsson, W. and Landelius, T. (2000), 'Effect of clouds on UV irradiance: As estimated from cloud amount, cloud type, precipitation, global radiation and sunshine duration', *Journal of Geophysical research, vol. 105, NO. D4, Pages 4927-4935* .

Kerr, J. B. and McElroy, C. T. (1993), 'Evidence for Large Upward Trends of Ultraviolet-B Radiation Linked to Ozone Depeletion', *Science, Vol 262, 12* .

Kerr, J. B. and Seckmeyer, G. (2003), 'Surface Ultraviolet Radiation: Past and Future', *World Meteorological Organisation, Scientific Assessment of Ozone Depletion: Global Ozone and Monitoring Project, Report No. 47, 5.1-5.46* .

Koepke, P., Backer, H. D., Bais, A., Curylo, A., Eerme, K., Feister, U., Johnsen, B., Junk, J., Kazantzidis, A., Krzyscin, J., Lindfors, A., Olseth, J. A., den Outer, P., Pribullova, A., Schmalwieser, A. W., Slaper, H., Staiger, H., Verdebout, J., Vuilleumier, L. and Weihs, P. (2006), 'Modelling solar UV radiation in the past: comparison of algorithms and input data', *Proc. of SPIE Vol. 6362 636215-2* .

Koepke, P., Reuder, J. and Schwander, H. (2002), 'Solar UV radiation and its variability due to the atmospheric components', *Devel. Photochem.Photobiol. 6: 11-34 ISBN: 81-7895-053-7* .

Kouwenberg, J. H. M., Browman, H. I., Cullen, J. J., Davis, R. F., St-Pierre, J.-F. and Runge, J. A. (1999a), 'Biological weighting of ultraviolet(280-400 nm) induced mortality in marine zooplankton and fish. I. Atlantic cod (Gadus morhua) eggs', *Marine Biology 134: 269-284* .

Kouwenberg, J. H. M., Browman, H. I., Runge, J. A., Cullen, J. J., Davis, R. F. and StPierre, J.-F. (1999b), 'Biological weighting of ultraviolet (280-400 nm) induced mortality in marine zooplankton and fish. II Calanus finmarchius (Copepoda) eggs', *Marine Biology 134: 285-293* .

Kuhn, P. S., Browmann, H. I., Davis, R. F., Cullen, J. J. and McArthur, B. L. (2000), 'Modeling the effects of ultraviolet radiation on embryos of Calcus finmarchicus and Atlantic cod (Gadus morhua) in a mixing environment', *Limnol. Oceanogr., 45(8), 1797-1806* .

Lindfors, A. V., Arola, A., Kaurola, J., Taalas, P. and Svenøe, T. (2003), 'Long-term erythemal UV doses at Sodankylä estimated using total ozone, sunshine duration, and snow depth', *Journal of Geophysical Research - Atmos. 108: Art. no. 4518 Aug. 28* .

Losey, G. S., Cronin, T. W., Goldsmith, T. H., Hyde, D., Marshall, N. J. and Mcfarland, W. N. (1998), 'The UV visual world of fishes: a review', *Journal of Fish Biology 54, 921-943* .

Madronich, S., McKenzie, R. L., Björn, L. O. and Caldwell, M. M. (1998), 'Changes in biologically active ultraviolet radiation reaching the Earth′s surface', *Journal of Photochemistry and Photobiology B: Biology 46, 5-19* .

Mayer, B., Kylling, A., Madronich, S. and Seckmeyer, G. (1998), 'Enhanced absorption of UV radiation due to multiple scattering in clouds: Experimental evidence and theoretical explanation', *Journal of Geophysical reasearch, vol. 103, No D23, pages 31, 241-31, 254* .

Melle, W. (1985), Predasjon på torskens egg og larver i Lofoten (Predation on cod eggs and larvae in the lofoten), Thesis in fisheries biology, University of Bergen.

met.no (2007), 'Meteorologisk Institutt', *www.met.no* .

Molina, M. and Rowland, F. (1974), 'Stratospheric Sink for Chlorofluoromethanes: Chlorine Atom-Catalysed Destruction of Ozone', *Nature 249: 810-2* .

Olseth, J. A. and Skartveit, A. (1989), 'Observed and modelled hourly luminous efficacies under arbritrary cloudiness', *Solar energy, 42, 221-233* .

Olseth, J. A. and Skartveit, A. (1993), 'Characteristics of hourly global irradiance modelled from cloud data', *Solar Energy Vol. 51, No. 3, pp. 197-204* .

Reuder, J., Ghezzi, F., Palenque, E., Torrez, R., Andrade, M. and Zaratti, F. (2007), 'Investigations on the effect of high surface albedo on erythemally effective UV irradiance: Results of a campaign at the Salar de Uyuni, Bolivia', *Journal of Photochemsitry and Photobiology B: Biology 87, 1-8* .

Reuder, J. and Koepke, P. (2005), 'Reconstruction of UV radiation over Southern Germany for the past decades', *Met. Zeitschrift, Vol. 14. No. 2, 237-246* .

Reuder, J. and Schwander, H. (1999), 'Aerosol effects on UV radiation in nonurban regions', *Journal of Geophysical reasearch, Vol. 104, NO. D4, pages 4065-4077* .

Ricchiazzi, P., Yang, S. R., Gautier, C. and Sowle, D. (1998), 'SBDART: A research and teaching software tool for plane-parallell radiative transfer in the Earth′s atmosphere', *Bulletin of the American Meteorological Society 79(10): 2101-2114* .

Ruggaber, A., Dlugi, R. and Nakajima, T. (1994), 'Modelling Radiation Quantities and Photolysis Frequencies in the Troposphere', *Journal of Atmospheric Cehmistry 18: 171-210* .

Sætre, O. (2006), Målt og modellert UV-stråling i Bergen, Master's thesis, University of Bergen.

Schwander, H., Kaifel, A., Ruggaber, A. and Koepke, P. (2001), 'Spectral radiative-transfer modeling with minimized computation time by use of a neural-network technique', *20 January 2001 / Vol. 40, No. 3 / Applied Optics* .

Schwander, H., Koepke, P., Kaifel, A. and Seckmeyer, G. (2002), 'Modification of spectral UV irradiance by clouds', *Journal of Geophysical research, vol. 107, NO. D16,4296, 10.1029/2001JD001297* .

Schwander, H., Koepke, P. and Ruggaber, A. (1997), 'Uncertainties in modeled UV irradiances due to limited accuracy and availability of input data', *Journal of Geophysical Research, Vol., 102, NO. D8, Pages 9419-9429* .

Seinfeld, J. H. and Pandis, S. (1998), *Atmospheric Chemistry and Physics*, John Wiley and Sons, Inc. New York.

Skreslet, S., Borja, A., Bugliaro, L., Hansen, G., Meerkotter, R., Olsen, K. and Verdebout, J. (2005), 'Some effects of ultraviolet radiation and climate on the reproduction of Clanus finmarchicus (Copepoda) and year class formation in Arcto-Norwegian cod (Gadus morhua)', *ICES Journal of Marine Science, 62: 1293-1300* .

Stenevik, E. K. and Sundby, S. (2007), 'Impacts of climate change on commercial fish stocks in Norwegian waters', *Marine Policy* **31**(19-31).

Sundby, S. (1983), 'A one-dimensional model for the vertical distribution of pelagic fish eggs in the mixed layer', *Deep-Sea Research, 30(6A):645-661* .

Sundby, S. (1991), 'Factors affecting the vertical distribution of eggs', *ICES mar. Sci. Symp. 192:33-38* .

Sundby, S. (2000), 'Recruitment of Atlantic cod stocks in relation to temperature and advection of copepod populations', *Sarsia 85: 277-298* .

Sundby, S., Bjørke, H., Soldal, A. V. and Olsen, S. (1989), 'Mortality rates during the early life stages and year class strength of northeast Arctic cod (Gadus morhua L)', *Rapp P. -v Réun Cons. int. Explor. Mer. 191:351-358* .

Sundby, S. and Bratland, P. (1987), 'Spatial distribution and production of eggs from Northeast-Arctic cod at the coast of northern Norway 1983-1985', *Fisken og Havet, 1:1-58* .

Sundby, S. and Nakken, O. (2007), Spatial shifts in spawning habitats of Arcto-Norwegian cod induced by climate changes.

Svenøe, T. (2000), Re-evaluation, statistical analysis and prediction based on the Tromsø total ozone record, PhD thesis, University of Tromsø.

UVAC project (2003), 'The influence of UVR and climate conditions on fish stocks: A case study of the northeast Artic cod', *Project coordinated by Dr. Georg Hansen, Norwegian Institute for Air Research (NILU), Tromsø, Norway* .

Wallace, J. M. and Hobbs, P. V. (1977), *Atmospheric Science - an introductory survey*, Academic Press.